ARISTOTLE UNIVERSITY OF THESSALONIKI
Interinstitutional Program of Postgraduate Studies in
PALAEONTOLOGY – GEOBIOLOGY

ANASTASIA KARAKOSTA
Geologist

SYSTEMATIC STUDY OF THE EARLY PLEISTOCENE *CANIS* (MAMMALIA, CANIDAE) FROM TSIOTRA VRYSSI (MYGDONIA BASIN, GREECE)

MASTER THESIS

DIRECTION: Macropalaeontology
Directed by: Aristotle University of Thessaloniki

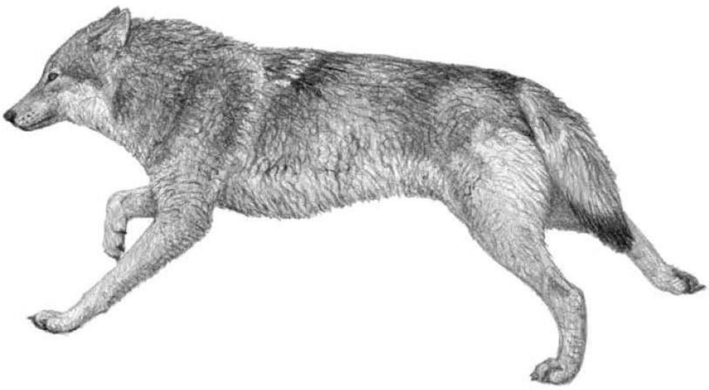

THESSALONIKI
2022

Interinstitutional Program of Postgraduate Studies in PALAEONTOLOGY – GEOBIOLOGY

supported by:

Τμήμα Γεωλογίας ΑΠΘ
School of Geology AUTh

Τμήμα Βιολογίας ΑΠΘ
School of Biology AUTh

Τμήμα Γεωλογίας & Γεωπεριβάλλοντος
ΕΚΠΑ

Faculty of Geology & Geoenvironment
NKUA

Τμήμα Γεωλογίας Παν/μίου Πατρών
Department of Geology, Patras Univ.

Τμήμα Γεωγραφίας Παν/μίου Αιγαίου
Department of Geography, Aegean Univ.

ANASTASIA KARAKOSTA
ΑΝΑΣΤΑΣΙΑ ΚΑΡΑΚΩΣΤΑ
Πτυχιούχος Γεωλόγος

SYSTEMATIC STUDY OF THE EARLY PLEISTOCENE *CANIS* (MAMMALIA, CANIDAE) FROM TSIOTRA VRYSSI (MYGDONIA BASIN, GREECE)

ΣΥΣΤΗΜΑΤΙΚΗ ΜΕΛΕΤΗ ΤΩΝ ΚΑΤΩ- ΠΛΕΙΣΤΟΚΑΙΝΙΚΩΝ *CANIS* (MAMMALIA, CANIDAE) ΑΠΟ ΤΗΝ ΑΠΟΛΙΘΩΜΑΤΟΦΟΡΟ ΘΕΣΗ ΤΣΙΟΤΡΑ ΒΡΥΣΗ (ΛΕΚΑΝΗ ΜΥΓΔΟΝΙΑΣ, ΕΛΛΑΔΑ)

Υποβλήθηκε στο ΔΠΜΣ Παλαιοντολογία-Γεωβιολογία

Ημερομηνία Προφορικής Εξέτασης: 03/03/2022
Oral Examination Date: 03/03/2022

Three-member Examining Board

Professor Dimitrios S. Kostopoulos, Supervisor
Professor Katerina Harvati, Member
Assistant Professor Sokratis Roussiakis, Member

Τριμελής Εξεταστική Επιτροπή

Καθηγητής Δημήτριος Κωστόπουλος, Επιβλέπων
Καθηγήτρια Αικατερίνη Χαρβάτη, Μέλος Τριμελούς Εξεταστικής Επιτροπής
Επίκουρος Καθηγητής, Σωκράτης Ρουσιάκης, Μέλος Τριμελούς Εξεταστικής Επιτροπής

External Assistant/Εξωτερικός Συνεργάτης (σύμφωνα με ΕΔΕ5/15-7-2019)
Dr. George E. Konidaris/ Δρ. Γεώργιος Ε. Κονιδάρης

SYSTEMATIC STUDY OF THE EARLY PLEISTOCENE *CANIS* (MAMMALIA, CANIDAE) FROM TSIOTRA VRYSSI (MYGDONIA BASIN, GREECE) – *Master Thesis*

ΣΥΣΤΗΜΑΤΙΚΗ ΜΕΛΕΤΗ ΤΩΝ ΚΑΤΩ- ΠΛΕΙΣΤΟΚΑΙΝΙΚΩΝ *CANIS* (MAMMALIA, CANIDAE) ΑΠΟ ΤΗΝ ΑΠΟΛΙΘΩΜΑΤΟΦΟΡΟ ΘΕΣΗ ΤΣΙΟΤΡΑ ΒΡΥΣΗ (ΛΕΚΑΝΗ ΜΥΓΔΟΝΙΑΣ, ΕΛΛΑΔΑ) – *Μεταπτυχιακή Διπλωματική Εργασία*

Citation:

Karakosta A., 2022. – Systematic study of the Early Pleistocene *Canis* (Mammalia, Canidae) from Tsiotra Vryssi (Mygdonia Basin, Greece). Master Thesis, Interinstitutional Program of Postgraduate Studies in Palaeontology-Geobiology. School of Geology, Aristotle University of Thessaloniki, 75 pp.

Cover Figure: Canis lupus, Mauricio Antón (Wang and Tedford, 2008)

Content

Acknowledgements

I would like to thank primarily my supervisor, Professor Dimitrios Kostopoulos for his notable guidance, along with his recommendations on the manuscript that favoured the completion of this Master thesis. Secondly, I express my gratitude to the members of the examining board; Professor Katerina Harvati, and Assistant Professor Sokratis Roussiakis, for their comments on the text. I am deeply thankful to Dr. George Konidaris, for his great assistance through this research that was in most aspects, instrumental. His suggestions on bibliographic sources, his active contribution and comments on the manuscript were most valuable. To MSc Anastasia Gkeme, I thank her for her friendly advice and provisions on bibliography from the very beginning of the research. I kindly thank Emer. Prof. George D. Koufos for always being accessible to share his helpful advice. Furthermore, I express my appreciation to the excavation team of Tsiotra Vryssi; Emer. Prof. George D. Koufos, Prof. Dimitris Kostopoulos, Prof. Katerina Harvati, Dr. George Konidaris, Dr. Vangelis Tourloukis, Dr. Domenico Giusti and Msc Nicholas Thompson, that discovered the studied material of this thesis. The excavations at Tsiotra Vryssi were supported by the European Research Council STG no. 283503 (PaGE) and the European Research Council CoG 724703 (CROSSROADS), both awarded to Professor Katerina Harvati. Finally, I am grateful to my fellow MSc students; Georgia Boni, Kristallia Chitoglou and Anastasia Katsagoni for the comradeship and encouragement through our research in the past year of the pandemic.

Abstract

The Lower Pleistocene site of Tsiotra Vryssi (TSR, Mygdonia basin, Greece), has revealed a rich late Villafranchian fauna in which canids are well-represented. The present thesis focuses on the systematic study of the canid (Mammalia, Carnivora, Canidae) material from TSR and its comparison with Early Pleistocene European taxa.

Three taxa have been recognized in the locality: two medium-sized canids (a larger and a smaller one) and a large-sized one. The larger medium-sized canid has been referred to as *Canis borjgali* vel *apolloniensis*, portraying many similarities with both *Canis borjgali* from Dmanisi (Georgia) and *Canis apolloniensis* from Apollonia-1 (Greece). The smaller medium-sized canid has been attributed to *Canis* sp. (morphotype B). Its overall morphology resembles the larger taxon, however its smaller size and some anatomical differences, set their in between relationships questionable and its species attribution unclear. Nevertheless, both TSR taxa are part of the early evolutionary stages of the *C. mosbachensis* lineage and are distinct from the more primitive *C. etruscus* and *C. arnensis*. The large-sized canid has been attributed to *Canis* (*Xenocyon*) sp. based on the general morphology and proportions of a single molar. The postcranial remains belong to medium-sized canids and have been attributed to *Canis* sp.; their study resulted in a notable metrical and morphological variability. Such variability could support the coexistence of two medium-sized species or just be part of intraspecific variation.

Περίληψη

Η Κάτω Πλειστοκαινική θέση της Τσιότρα Βρύσης (TSR, λεκάνη Μυγδονίας, Ελλάδα), έχει αποκαλύψει μια πλούσια πανίδα του άνω Βιλαφραγκίου στην οποία οι κυνίδες αντιπροσωπεύονται επαρκώς. Η παρούσα εργασία εστιάζει στη συστηματική μελέτη του υλικού των κυνίδων (Mammalia, Carnivora, Canidae) από την Τσιότρα Βρύση και στη σύγκρισή του με ευρωπαϊκά είδη του Κάτω Πλειστόκαινου.

Στη θέση έχουν αναγνωριστεί τρία είδη: δύο κυνίδες μεσαίου μεγέθους (ένας μεγαλύτερος και ένα μικρότερος) και ένας μεγάλου μεγέθους. Ο μεγαλύτερος κυνίδης μεσαίου μεγέθους αναφέρεται ως *Canis borjgali* vel *apolloniensis*, καθώς παρουσιάζει πολλές ομοιότητες τόσο με τον *Canis borjgali* από το Dmanisi (Γεωργία) όσο και με τον *Canis apolloniensis* από την Απολλωνία-1 (Ελλάδα). Ο μικρότερος κυνίδης μεσαίου μεγέθους έχει αποδοθεί στο *Canis* sp. (morphotype B). Η συνολική μορφολογία του μοιάζει με το μεγαλύτερο, ωστόσο το μικρότερο μέγεθος και ορισμένες ανατομικές διαφορές καθιστούν αμφισβητήσιμη τη μεταξύ τους σχέση και ασαφή την απόδοση του είδους του. Παρόλα αυτά, και τα δύο είδη της Τσιότρα Βρύσης αποτελούν μέρος των πρώιμων εξελικτικών σταδίων της γραμμής του *C. mosbachensis* και διαφέρουν από τα πιο πρωτόγονα *C. etruscus* και *C. arnensis*. Ο μεγάλου μεγέθους κυνίδης έχει αποδοθεί στο *Canis* (*Xenocyon*) sp. με βάση τη γενική μορφολογία και τις αναλογίες ενός μόνο δείγματος. Ο μετακρανιακός σκελετός ανήκει σε κυνίδες μεσαίου μεγέθους και αποδόθηκε στο *Canis* sp. Από τη μελέτη του διαπιστώθηκε σημαντική μετρική και μορφολογική ποικιλομορφία, η οποία θα μπορούσε να υποστηρίξει τη συνύπαρξη δύο μεσαίου μεγέθους ειδών ή απλώς να αποτελεί μέρος ενδοειδικής ποικιλότητας.

1. Introduction

The family Canidae Fischer von Waldheim, 1817 which is one of the oldest families of the order Carnivora Bowditch, 1821, appeared during the Late Eocene (40–37 Ma) in North America. Today, around 36 living canid species are known, all belonging to the Caninae subfamily (Sillero Zubiri, 2009; Zrzavý et al. 2018). Canids are characterised by an elongated snout and an unreduced dental formula of 3143-2/314-2 (Wang et al., 2004). As carnivorans, they possess a pair of carnassial teeth (last upper premolar, P4/first lower molar, m1) (e.g., Bellani, 2020). An additional anatomical feature that defines canids is the entotympanic bulla, which is inflated and partially divided by an internal septum (Wang and Tedford, 1994, 2007).

1.1 Plio-Pleistocene *Canis* representatives of Europe

During the Late Miocene *Eucyon* (Tribe Canini, Caninae) invaded Eurasia and its dispersion was rather simultaneous in the Old World (Sotnikova and Rook, 2010). *‘‘Canis’’ cipio* (Crusafont, 1950) from Concud and Los Mansuetos (Turolian, Spain) is the oldest European record of the Canini, represented by scarce material (Sotnikova and Rook, 2010). Wang and Tedford (2007) assume that this canid could be better ascribed to *Eucyon* than to *Canis*. Despite its successful Early Pliocene dispersion, *Eucyon* became extinct during the Late Pliocene (early Villafranchian).

Canis ferox is the first species of *Canis* appearing in the Late Miocene–Early Pliocene of North America. It stands morphologically between *E. davisi* and *Canis lepophagus* (Tedford et al., 2009). The evolution of *Canis* in America continued with *C. edwardii*, related to the coyote group, and *C. armbrusteri* which is probably of Eurasian descendance. In Asia the oldest known *Canis* is *Canis* cf. *etruscus* from Yushe Basin (China), around 3.4 Ma (e.g., Sotnikova and Rook, 2010).

The dispersal traces of the genus *Canis* in Europe in the Early Pleistocene, around 2.0–1.8 Ma, have been referred to as the “wolf event” (Azzaroli, 1983), associated with the middle to late Villafranchian faunal transition. However, the presence of *Canis* sp. in the Late Pliocene (early Villafranchian) locality of Vialette (France), sets the earliest *Canis* record in western Europe around 3.14 Ma (Lacombat et al., 2008). Additional material from the middle Villafranchian Coste San Giacomo (Italy), around 2.1 Ma, referred to as *Canis* cf. *etruscus*, shows that the “wolf event”, was not appropriate to mark the faunal turnover (Sardella and Palombo, 2007, Sotnikova and Tedford, 2010). Therefore, the “*Pachycrocuta brevirostris* event”, i.e. the arrival of this giant hyena in Europe, has been suggested by Martínez-Navarro (2010) to better label the transition at ~2.0 Ma.

The *Canis* guild towards the end of the middle and the beginning of the late Villafranchian in Europe is characterised by the presence of three species: the medium-sized *Canis etruscus* and *C. arnensis*, and the large-sized *Canis* (*Xenocyon*) *falconeri*.

Canis etruscus Forsyth Major, 1877 is best recorded in the Italian sites of Olivola, Upper Valdarno (Poggio Rosso; Tasso) and Pantalla (Torre, 1967, Rook, 1993, Cherin et al., 2014) around 2.0–1.8 Ma, and has been also described in Fonelas P1 (Spain), Gerakarou-1 and Apollonia-1 (Greece) (Garrido, 2008; Koufos, 1992, 2001, 2018). This canid displays some unique characteristics, especially the larger skull length compared to the rest of the species. It has been suggested by many authors (e.g., Torre 1967; Sotnikova and Rook, 2010) that it is the ancestor of *C. mosbachensis* and subsequently of *C. lupus*. *Canis arnensis* Del Campana, 1913 is mostly recorded in the Italian sites of Poggio Rosso and Tasso, and additionally in Senèze (France) and Gerakarou-1 (Greece). It is smaller compared to *C. etruscus*, and it has been associated with the coyotes and jackals in the past (e.g., Kurtén, 1974). The coexistence of *C. arnensis* and *C. etruscus* is undoubtful, however, the relationships between them are yet unclear (e.g., Cherin et al., 2014).

The large-sized *C.* (*X.*) *falconeri*, Forsyth Major, 1877 is a hypercarnivorous canid that has been recorded in a few European localities, especially in the Upper Valdarno. The taxonomy of *Canis* (*Xenocyon*) is complicated and thus several names have been suggested in the literature to describe it. Martínez-Navarro and Rook (2003) attributed this large-sized and hypercarnivorous canid from Europe to the genus *Lycaon* due to its resemblance to the extant African hunting dog *Lycaon pictus*. Molecular systematics resulted in that *Lycaon* and *Cuon*, two large-sized hypercarnivorous canids, are in fact sister taxa belonging to the *Canis* group (Gopalakrishnan et al., 2018, Bartolini Lucenti et al., 2021). In the present work the neutral term of *Xenocyon* is used, as suggested in the recent works of Bartolini Lucenti et al. (2021) and Madurell-Malapeira et al. (2021).

Canis accitanus, was identified by Garrido and Arribas (2008), in the Spanish locality of Fonelas- P1 (2.0–1.8 Ma). Its small size and several dental features led to its attribution as a separate species, but it has been debated in the literature. Brugal and Boudadi-Maligne (2011) suggest that it rather belongs to *C. arnensis* based on its size, whereas Martínez-Navarro et al. (2021) argue that it could be within the intraspecific variability of *C. etruscus*, which is also present in the site.

The *Canis* material from Dmanisi (~1.8 Ma, Georgia) was originally attributed to *C. etruscus* (Vekua, 1995), but was recently identified as belonging to the new species *C. borjgali* (Bartolini Lucenti et. al., 2020). *Canis borjgali* stands morphologically between *C. etruscus* and *C. mosbachensis* but is closer to the latter. This new species seems to change the previously established phylogenetic condition within the *C. lupus* lineage and is proposed to be the ancestor of *C. lupus* instead of the more primitive *C. etruscus* (Bartolini Lucenti et al., 2020).

Canis orcensis is also a newly ascribed species from Venta Micena, ~1.6 Ma (Spain) (Martínez-Navarro et al., 2021). This canid most resembles *C. borjgali*, *C. mosbachensis* and *C. apolloniensis*, and is described as a chrono-species between the primitive and the most derived ones. *Canis apolloniensis* from Apollonia-1, ~1.3–1.0

Ma (Greece), was first recognised by Koufos and Kostopoulos (1997) while additional material was described later by Koufos (2018). Its morphology is also closer to the *C. mosbachensis* lineage. Madurell-Malapeira et al. (2021) suggests that *C. orcensis* and *C. apolloniensis* could be attributed to *C. mosbachensis*, pushing back the first occurrence of this taxon as far as ~1.6 Ma.

Canis mosbachensis was first described by Soergel, 1925 from Jockrim, 600–500 ka (Germany). It was widely dispersed in Europe during late Early–Middle Pleistocene, recorded in several sites, e.g., Vallparadís, Cueva Victoria (Spain), Pirro Nord (Italy) and Untermassfeld (Germany) (Sotnikova 2001; Petrucci et al. 2013; Bartolini Lucenti et al., 2017). It is a controversial medium-sized species, very close to *C. lupus* and is often considered as its direct ancestor (e.g., Sardella et al., 2014). However, it has been also questioned whether it is a distinct species or instead a subspecies of *C. lupus* (e.g., Thenius, 1954) or of *C. etruscus* (e.g., Bonifay, 1971). *Canis* (*Xenocyon*) *lycaonoides* (Kretzoi, 1938) is an advanced hypercarnivorous canid that replaced the previous *C.* (*X.*) *falconeri*. Its spread was rather simultaneous with *C. mosbachensis* in Europe and it was widely distributed, e.g., Pirro Nord, Untermassfeld, Apollonia-1 and Dmanisi (e.g., Bartolini Lucenti et al. 2017, 2021).

The Lower Pleistocene locality of Tsiotra Vryssi has revealed rich and important canid material that has not been systematically examined so far. The present thesis offers an initial systematic study of the TSR canid specimens with the aim of contributing further to the taxonomy and evolution of *Canis* in Europe during the Early Pleistocene.

1.2 Geological setting

Mygdonia Basin is located northeast to Thessaloniki in Central Macedonia, Greece. The fossiliferous localities of the basin are known since the end of the 1970s, with extensive fieldwork being carried out over the years. The discovery and study of numerous fossils has enriched the Pleistocene mammal fossil record of Greece and the Mygdonia Basin is considered today an important European reference region (Koufos et al., 1995; Koufos, 2001; Konidaris et al., 2015).

The Mygdonia Basin (Fig. 1) is an elongated East-West- trending tectonic depression extended to a wide area. Its formation started during the Early–Middle Miocene with the development of the Pre-Mygdonia Basin, which was filled with fluvial-fluviotorrential and lacustrine sediments during Neogene–Early Pleistocene times. The central and eastern basement of the basin consists of metamorphic rocks (schists, gneisses, amphibolites) of the Serbomacedonian Massif while the western part is developed on slightly metamorphosed sediments (phyllites, limestones, sandstones), belonging to the Circum-Rhodope Belt (Kockel et al., 1977). At the beginning of the Middle Pleistocene, new tectonic activity led to the division of Pre-Mygdonia basin into smaller basins (Mygdonia, Zagliveri, Marathousa, Doubia) that were filled mainly by lacustrine deposits. The Mygdonia basin developed into a large lake during the Pleistocene which today is represented by the remnant lakes of Volvi and Koronia (Psilovikos 1977; Koufos et al., 1995).

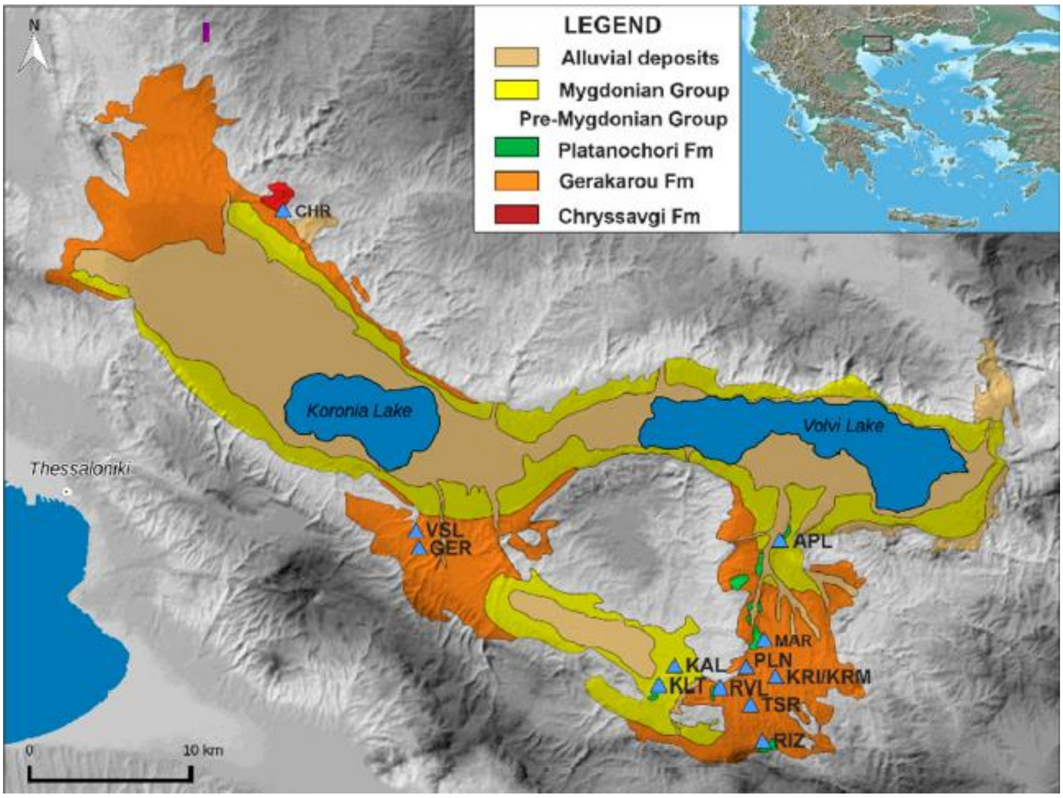

Figure 1. Geological map with the Neogene and Quaternary lithostratigraphic units, and the fossiliferous localities of the Mygdonia Basin (Konidaris et al., 2021; modified from Konidaris et al., 2015; data from Koufos et al., 1995).

The Neogene and Quaternary deposits have been divided into two main lithostratigraphic units, the Pre-Mygdonian Group (Neogene to Early Pleistocene) and the Mygdonian Group (Middle Pleistocene to Holocene) (Psilovikos, 1977; Koufos et al., 1995). The Pre-Mygdonian Group consists of three successive formations (Fm): Chrysavgi Fm, Gerakarou Fm and Platanochori Fm (Koufos et al., 1995). Gerakarou Fm in particular, is the most widely exposed formation of Mygdonia Basin, more than 100 m thick, with typical exposures near Gerakarou village. The Formation mainly consists of red beds that form alternating lenses and lens-shaped beds of loose gravels, sands and red-brown silts and clays deposited in a fluviotorrential environment (Koufos et al., 1995). The known fossiliferous localities found in the upper part of the Gerakarou Fm are Gerakarou-1 (GER), Vassiloudi-1 (VSL), Krimni-1, 2 and 3 (KRI, KRM, KMN), Kalamoto-2 (KLT) and Tsiotra Vryssi (TSR). The study of their faunas indicates a late Villafranchian (Early Pleistocene) age, even though the localities are not isochronous (Koufos et al., 1995; Tsoukala and Chatzopoulou, 2005; Konidaris et al., 2015, 2021; Kostopoulos et al. in press).

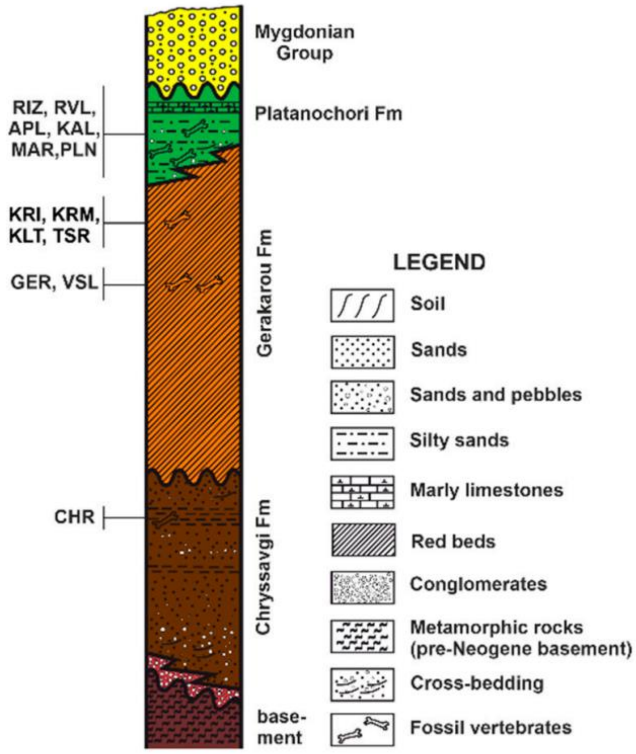

Figure 2. Simplified composite stratigraphic column of the Mygdonia basin (Konidaris et al., 2021; data from Koufos et al., 1995).

1.2.1 Tsiotra Vryssi

The fossiliferous site of Tsiotra Vryssi (TSR) was discovered in 2014 during a field survey led by a team of researchers from the Aristotle University of Thessaloniki and Eberhard Karls University of Tübingen. TSR is located in the Marathousa sub-basin, southwest of Krimni and north of Riza village, and it is placed in the upper levels of the Gerakarou Fm. The fossiliferous layer at Tsiotra Vryssi consists of sandy silts and has a thickness of ~1 m (Giusti et al., 2019). Since the discovery of the site, systematic excavations revealed a significant number of large mammal fossils accompanied by some micromammals, reptiles, and birds (Konidaris et al., 2015, 2021). Fossils have been discovered either isolated or as anatomically connected skeletal elements. The preliminary faunal list of the large mammals for TSR is given in Table 1.

A late Villafranchian age has been suggested for the TSR fauna based on several lines of biochronological evidence (Konidaris et al., 2015, 2021), such as the presence of the large-sized hyaenid *Pachycrocuta brevirostris,* a species that invaded Europe around 2.0 Ma ("*Pachycrocuta brevirostris* event" *sensu* Martínez-Navarro, 2010). The strongest indicator yet, is the co-existence of the two large-sized bovids, *Leptobos* and *Bison*. The age has been recently further constrained by Konidaris et al. (2021), based on magnetostratigraphy and cosmogenic radionuclides, and resulted in an age between 1.78 and ~1.5 Ma (within the first part of the late Villafranchian).

Table 1. Preliminary faunal list of the large mammals from Tsiotra Vryssi (Konidaris et al., 2021).

Order	Family	Genus	Species
Proboscidea	Elephantidae	*Mammuthus*	*meridionalis*
Carnivora	Canidae	*Canis*	sp.
	Ursidae	*Ursus*	*etruscus*
	Hyaenidae	*Pachycrocuta*	*brevirostris*
	Felidae	*Megantereon*	sp.
Perissodactyla	Equidae	*Equus*	sp. (medium-sized)
		Equus	sp. (large-sized)
	Rhinocerotidae	*Stephanorhinus*	sp.
Artiodactyla	Giraffidae	*Palaeotragus*	sp.
	Cervidae	*Cervus*	sp.
		Praemegaceros	sp.
	Bovidae	*Pontoceros*	sp.
		Leptobos	sp.
		Bison	cf. *degiulli*

2. Materials and methods

The systematic study of the Early Pleistocene *Canis* from Tsiotra Vryssi is based on the study of craniodental and postcranial material. The material is stored at the Museum of Geology-Palaeontology-Palaeoanthropology of the School of Geology, Aristotle University of Thessaloniki (LGPUT). Comparative material has been used from the Mygdonia Basin localities (Koufos, 1987, 2018; Koufos and Kostopoulos, 1997) and relevant literature (e.g., Bonifay, 1971; Rook, 1993; Sotnikova, 2001; Garrido and Arribas, 2008; Petrucci et al., 2013; Cherin et al., 2014; Bartolini Lucenti, 2015; Bartolini Lucenti et al., 2017; Martinez-Navarro et al., 2021).

The systems of measurements for cranial, dentognathic and postcranial skeleton follow von den Driesch (1976) and they are slightly modified (Figs. 4–7). Dental terminology (Fig. 3) follows Biknevicius and Van Valkenburgh (1996) as modified by Bartolini Lucenti (2015). The description of the postcranial skeleton terminology generally follows Miller (1964).

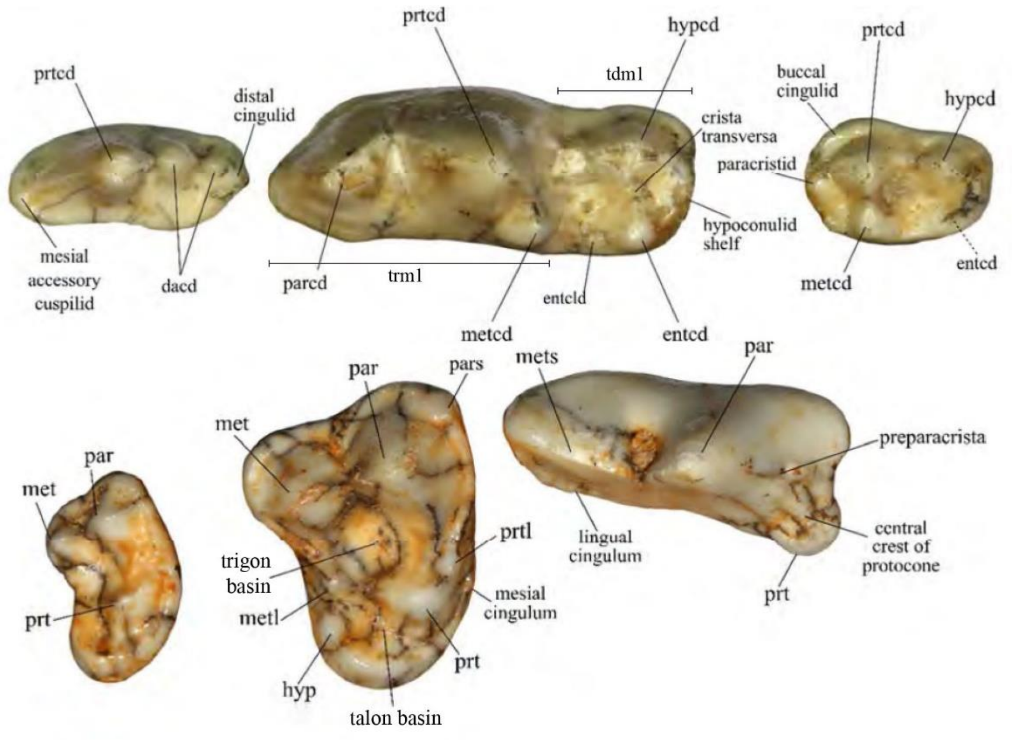

Figure 3. Dental terminology for lower and upper teeth in *Canis*. Modified from Bartolini Lucenti (2015). (for abbreviations see: page 21)

Measurements were taken with a digital caliper at 0.1 mm precision and they are presented in Tables 5–13 (Appendix I). Data were analysed using PAST 3.26 software (Hammer et al., 2001). Simpson's log ratio diagrams (Simpson, 1941; Simpson et al., 1960) were performed in Microsoft Excel. For the principal component analysis (PCA), data were log-transformed following Mosimann's method (Mosimann, 1970); each value is divided by the geometric mean of all specimen's variables and then the results are logarithmized.

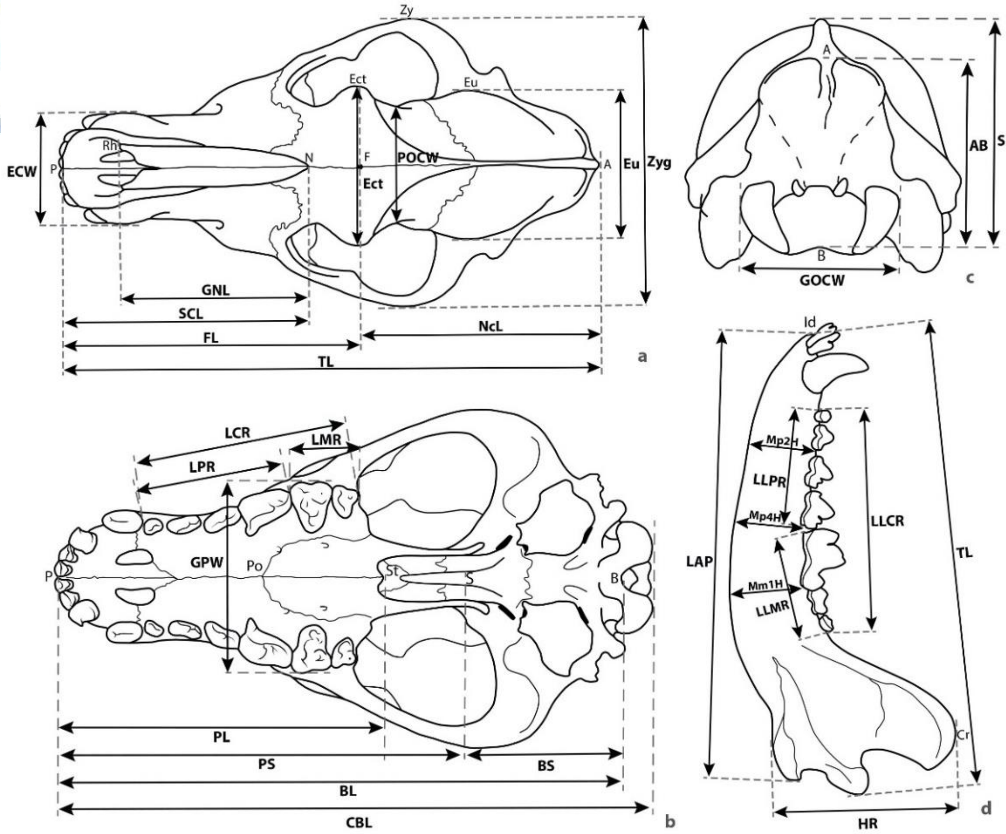

Figure 4. Cranial and mandibular measurements. **a**. Cranium, ventral view; **b**. Cranium, dorsal view; **c**. Cranium, caudal view; **d**. Mandible, lateral view. Modified from von den Driesch (1976). (for abbreviations see: page 21)

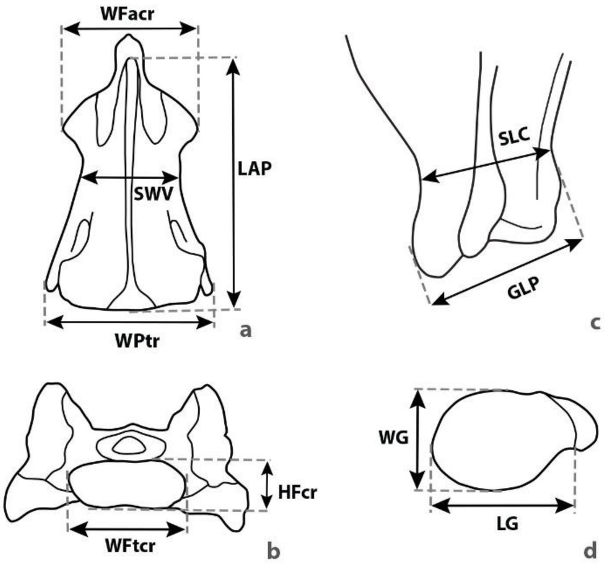

Figure 5. Measurements of vertebrae and scapula, following Von den Driesch (1976). **a**. Axis, dorsal view; **b**. Sacrum, posterior view; **c**. Left scapula, lateral view; **d**. Right scapula, distal view. b and c modified from von den Driesch (1976). (for abbreviations see: page 21)

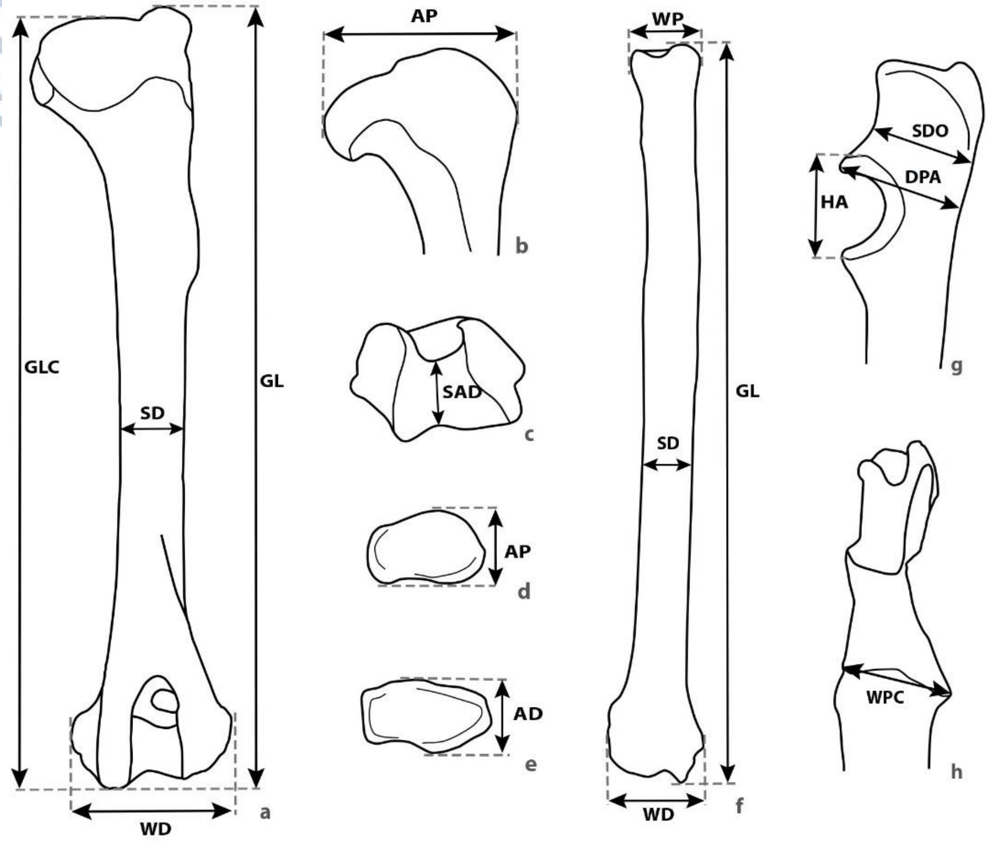

Figure 6. Postcranial skeletal measurements. **a**. Right humerus, posterior view; **b**. Right humerus, lateral view; **c**. Right humerus, distal view; **d**. Right radius, proximal view; **e**. Right radius, distal view; **f**. Right radius, anterior view; **g**. Right ulna, medial view; **h**. right ulna, anterior view. (for abbreviations see: page 21)

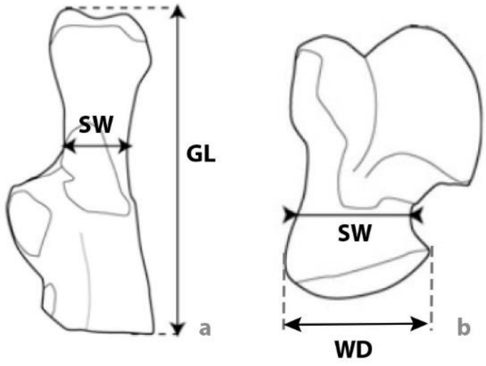

Figure 7. Measurements of the calcaneus and astragalus. **a**. Left calcaneus, anterior view; **b**. Astragalus, anterior view. Modified from Boudadi-Maligne (2010). (for abbreviations see: page 21)

Abbreviations

The abbreviations are a combination of Bartolini Lucenti (2015), Bartolini Lucenti et al. (2020), Sotnikova (2001) and Von den Driesch (1976).

Cranium

Tl: Total length of the cranium (prosthion–akrokranion); **FL**: Facial length (prosthion–frontal midpoint F); **NcL**: Neurocranium length (frontal midpoint–akrokranion); **SCL**: Splanchnocranium length (prosthion–nasion); **GNL**: Greatest length of the nasals (nasion–rhinion); **ECW**: External canine alveoli width; **Ect**: Frontal width (ectorbitale–ectorbitale); **POCW**: least width at the postorbital constriction; **Eu**: Greatest neurocranium width (euryon–euryon); **Zyg**: Zygomatic width (zygion–zygion); **CBL**: Condylobasal length of the cranium (prosthion–occipital condyles); **BL**: Basal length (prosthion-basion); **PS**: Basifacial axis (prosthion-synsphenion); **BS**: Basicranial axis (basion-synsphenion); **PL**: Palatal length (prosthion–staphylion); **GPW**: Greatest palatal width; **LCR**: Length of cheektooth row (P1–M2); **LMR**: Length of the molar row (M1–M2); **LPR**: Length of the premolar row (P1–P4); **AB**: Height of the occipital triangle (Akrokranion–Basion); **SH**: Cranium height (basioccipital–highest elevation of the sagittal crest); **GWOC**: Greatest width of the occipital condyles.

Mandible

TL: Total length (condyle process–infradentale); **LAP**: Length (angular process–infradentale); **HR**: Height of the ramus (basal point of the angular process–coronion); **LLCR**: Length of the cheektooth row (p1–m3) **LLPR**: Length of the premolar row (p1–p4); **LLMR**: Length of the molar row (m1–m3); **Mp2H**: Corpus height distal to p2 alveolus; **Mm1H**: Corpus height distal to m1 alveolus; **Mp4H**: corpus height distal to p4 alveolus.

Dentition

The upper teeth are indicated by upper case letters and the lower teeth by lowercase letters. **L**: mesiodistal length; **W**: buccolingual width; **prt**: protocone; **prtl**: protoconule; **hyp**: hypocone; **met**: metacone; **metl**: metaconule; **mets**: metastyle; **par**: paracone; **pars**: parastyle **prtcd**: protoconid; **parcd**: paraconid; **metcd**: metaconid **hypcd**: hypoconid; **entcd**: entoconid; **entld**: entoconulid; **dacd**: distal accessory cuspilid(s); **dac**: distal accessory cuspid(s); **tdm1**: talonid of m1; **trm1**: trigonid of m1.

Postcranial skeleton

GL: Greatest length; **SD**: Smallest width of the diaphysis; **AP**: Anteroposterior diameter of proximal end; **WP**: greatest width of proximal end; **AD**: Anteroposterior diameter of distal end; **WD**: greatest width of distal end; **WFacr**: Width of the *facies articularis cranialis*; **SWV**: Smallest width of the vertebra; **WPtr**: Width across the processus transversi; **LAP**: Length of the arch (including the *processus articulares* *caudales*); **SLC**: Smallest length of the *collum scapulae* (neck of the scapula); **GLP**: Greatest length of the *processus articularis*; **LG**: Length of the glenoid cavity; **WG**: Width of the glenoid cavity; **GLC**: Greatest length from caput; **SAD**: Smallest anteroposterior diameter of the trochlea; **SDO**: Smallest depth of the olecranon; **DPA**: Depth across the *processus anconaeus*; **WPC**: Width across the coronoid process; **HA**: Height of the articular surface; **WFtcr**: Width of the *facies terminalis cranialis*; **HFcr**: Height of the *facies terminalis cranialis*; **WS**: Shaft width in the middle; **SW**: Smallest width.

3. Systematic Palaeontology

Order Carnivora Bowditch, 1821

Family Canidae Fischer von Waldheim, 1817

Subfamily Caninae Fischer von Waldheim, 1817

Genus *Canis* Linnaeus, 1758

3.1 *Canis borjgali* vel *apolloniensis*

3.1.1 Material

Cranium and cranial fragments: TSR-D17-37a, cranium; TSR-G16-46 left cranial fragment with P2, P3, M1 and M2.

Upper dentition: TSR-D16-14, left P4 with broken protocone; TSR-G16-29, right P4; TSR-C15-13, right C; TSR-D17-42, left C; TSR-D14-7, fragmented right M2; TSR-E22-6, left I3.

Mandible: TSR-D17-37b, complete mandible; TSR-F14-2 right hemimandible with p1, p2, p4 and m1; TSR-H20-1, left fragmented hemimandible with m1 and m2.

3.1.2 Description

Cranium: TSR-D17-37a (Pl. I) is a well preserved, slightly deformed (dorsoventrally compressed) cranium with a broken left zygomatic. It is modestly elongated with elongated nasals that probably end beyond the maxillofrontal suture. The braincase, although deformed, seems well-developed, and so is the sagittal crest. The nuchal crest forms a relatively blunt/ triangular outline which is ventrally inclined. In lateral view, the profile looks smooth due to the deformation. The infraorbital foramen is placed above and distally to the P3, and it is slightly wide (the maxilla is curved at this area). In ventral view, the cranium has an almost complete dentary (only the left C is missing) and the toothrow is curved at the area of P3–P4. No diastemas occur between the premolars, but there is one between I3–C. The incisive foramen is elongated and seems to reach the distal part of the canine. The preserved left tympanic bulla is moderately inflated, oval shaped and the medial wall slightly deviates from the right one. The postglenoid processes are strong and the basioccipital area forms a sharp crest in the middle.

Upper dentition (Pls. I, III): The I1 and I2 present two accessory cuspids on both sides. The I3 is a canine-form tooth; it is larger than the other two incisors, and has a basal cingulum. The C is long, buccolingually compressed and curved. The P1 is large, conical, single rooted with a very small buccodistal cuspid and a mesialingual crista. The P2 and P3 are both buccolingually compressed and double rooted; they are similar to each other, with P3 being larger. The P2 has a small distal cuspid. The P3 bears at least one distal cuspid and deviates slightly from P2 and P4. The P4 is the largest and longest premolar. It has a high paracone and a sharp, not very straight metastyle. The protocone is individualised and modestly developed and is placed at the level of the mesial margin of the tooth (not so elevated and pointed in TSR-D17-37a, but in TSR-D16-14, TSR-G16-29 they are sharp and well-developed). A strong preparacrista runs the tooth at the mesial part and joins the central crest of the protocone (not in TSR-D17-37a). The distolingual cingulum is strong. The M1 has a larger and higher paracone compared to the metacone. The M1 protocone is well-developed and is separated from the metaconule. Due to dental wear, it is not possible to identify if the tooth bears a protoconule. The hypocone is not distinct on the cingulum but there is a small mesiolingual cuspid. The trigon basin is slightly deeper and larger than the talon basin. The cingulum at the buccal side is strong and expands distally and mesially. The M2 is buccolingually elongated but tends to be squared. The paracone of the M2 is larger than the metacone and the protocone is well-developed although slightly worn. No hypocone is visible on the lingual cingulum. The cingulum is strong on the buccal side. The trigon and talon basins of the M2 are shallow but the first one is better developed. The space between M1–M2 is narrow.

Mandible (Pls. I, III): The preserved mandibles have a rather low and normally thick corpus. There are two mental foramina on the buccal side, the larger one is located below p1 and the smaller one below the mesial part of p3. The masseteric fossa is deep and the coronoid process is tall (where preserved) and distally inclined. The condyle process of the specimen TSR-H20-1 appears to be slightly lower positioned contra to the rest specimens. The articular condyle is lingually inclined. In dorsal view, the toothrow is curved, especially at the area of p4–m1. A diastema is only present between c–p1**.**

Lower dentition (Pls. I, III): The incisors increase in size from i1 to i3 but remain small. The i2 and i3 have a distal accessory cuspid, whereas i1 does not. The canine is elongated and distally curved. The p1 is a conical single rooted tooth. The p2, p3, p4 are all buccolingually compressed, double rooted with high protoconids that are also distally inflated; especially the p4. The p2 lacks any accessory cuspids. The p3 is slightly larger than the p2 and has a small distal accessory cuspid, while there may be a small one on the distal cingulid. The p3 protoconid is lower than those of p4 and p2 and the alveoli seems to have a lower position, especially distally. The p4 is the largest premolar with a high protoconid and two distal cuspids: a well-developed one close to the protoconid and a smaller distal one (slightly visible). It also has a mesial crest on the protoconid, which is more distinct than in the other premolars. The protoconid of p4 is shorter than the m1 paraconid. The m1 is large, mesiolingually elongated and has a well-developed, high and distally curved protoconid. At the mesial part, the paraconid has a distally inclined mesial margin. The well-developed metaconid is found distolingually of the protoconid. In the talonid, the hypoconid is larger than the entoconid. These cusps are connected with a rather sinuous transverse crest. The basin is moderately deep and slightly lingually placed. An entoconulid is present distolingually, between the metaconid and the entoconid, but it is very small and slightly visible. The hypoconulid shelf at the very distal portion is worn and it is not clearly visible, while no other accessory cuspids can be seen for the same reason. The shape of the m2 tends to be elliptical with a broader mesial part compared to the less developed distal one. On the mesial part, the metaconid is smaller than the protoconid. A hypoconid is located distobuccally and is smaller than the metaconid and the protoconid, but it is typically developed. Distolingually, any entoconid is absent on the cingulum. The cingulum is well-developed mesiobuccally and distolingually. The m3 is oval shaped with a well-developed cingulum. Two small cuspids are visible mesially; the buccal one is slightly smaller than the lingual one.

3.2 *Canis* sp. (morphotype B)

3.2.1 Material

Cranium and cranial fragments: TSR-G20-11a cranium missing right I1, left I1, right I2, left I2, left I3 and left C.

Upper dentition: TSR-G20-11d, left C; TSR-G20-11e left I3; TSR-G20-11c; left I2.

Mandible: TSR-G20-11b, left hemimandible with c, p2, p3, p4, m1 and m2.

All above specimens belong to the same individual; the isolated upper teeth are those missing from the cranium, and were found in very close proximity to it.

3.2.2 Description

Cranium: TSR-G20-11a (Pl. II) is generally a well-preserved cranial specimen, slightly deformed on both dorsoventral and lateral sense. It is elongated with a moderately elongated snout. The deformation prohibits the identification of some features. The nasal bones are moderately elongated, and they prolong caudally beyond the maxillofrontal suture. The braincase is inflated although deformed. In lateral view, the height seems to increase gradually up to the frontal bone. The infraorbital foramen is narrow and is found above the P3. The sagittal crest is broken (not so developed on the preserved parts) but the occipital is developed with a blunt outline on the nuchal crest and is weakly inclined dorsally. In ventral view, the toothrow is gradually curved. Diastemas are present between P1–P3 and between I3–C. The incisive foramina are elongated and close before the distal part of the canine. The tympanic bullae are well-developed (the right one is damaged), oval-shaped but it is not clear if their medial walls are parallel to each other. The postglenoid processes are rather thin and the presphenoid area is broken. The basioccipital area is rather smooth and does not form a sharp ridge in the middle.

Upper dentition (Pl. II): The teeth are generally slender- delicate. The I2 is small and bears two small accessory cuspids on its medial and lateral sides. The I3 is canine-form possessing a cingulum on the base and a crista distally. The upper canine is long, curved and buccolingually compressed. The P1 is single cusped and single rooted. The P2 and P3 are both double rooted, mesiodistally elongated and similar to each other, but the P3 is larger. The P2 and P3 protocones are high and the P3 has two small distal accessory cusps. P1–P3 have a crista mesiolingually, which joins the basal cingulum lingually. The P3–P4 seem to be in line. The P4 is a distinctive carnassial with a high paracone and a sharp and shorter metastyle. The protocone is weakly developed and is placed at the level of the mesial margin. The preparacrista on the mesial margin is not very pronounced and the central crest of the protocone is not visible. The cingulum is strong distolingually. The paracone of the M1 is larger than the metacone. The protocone is well-developed and separated from the smaller protoconule and the metaconule. The hypocone is small but visible on the cingulum. The trigon basin is deeper than the talon one and slightly larger. The buccal cingulum is strong and expands distally and mesially. The lingual margin of the M1 is rather high and bended. The M2 is buccolingually elongated and has three distinct cusps. The paracone is larger than the metacone. The protocone is shorter but well-developed. The trigon and talon basins are shallow. The cingulum is strong buccolingually and present all around the tooth. M1–M2 space is somehow wide.

Mandible: TSR-G20-11b (Pl. II) is a right hemimandible, generally well-preserved, though the coronoid process is broken. The masseteric fossa, even though fragmented, can be described as rather shallow. The condyloid process is slightly lingually inclined and rather short. The rostral part of the hemimandible is missing (broken in front of the c) and the incisors are lacking. Two mental foramina are present, the larger one below the distal part of p1 and the mesial part of p2 and the smaller one is below the diastema between p2–p3. The corpus is slender and in dorsal view, the toothrow is curved.

Lower dentition (Pl. II): The three incisors are missing in TSR-G20-11b. The lower canine is elongated and distally curved. A diastema exists between c–p1, whereas very short diastemata are observed between the premolars p2–p4. The p1 is missing. The rest of the premolars are buccolingually compressed and double rooted. The p2 has a well-developed protoconid and lacks any distal cuspid. The p3 is slightly larger than the p2 and it possesses a small but visible distal accessory cuspid; an additional small cuspid may be present on the cingulum. The p3 alveoli is slightly deeper in the mandible compared to the p2 and p4. The p4 is the largest premolar and it is more inflated distally than the others. The protoconid is well-developed and it has two distal cuspids; a large one closer to the protoconid and a smaller one only slightly visible. A mesial crista on the protoconid is present on all premolars, but it is more pronounced on the p4. The protoconid of p4 is slightly shorter than the m1 paraconid. The m1 has a well-developed and high protoconid and a paraconid at the mesial side with a distally inclined mesial margin. The metaconid is located distolingually behind the protoconid and is well developed and distally inclined. In the talonid, the hypoconid is larger than the entoconid and they are connected with a sinuous transverse crest. The basin is deep and slightly lingually placed. The entoconulid is present distolingually, between the metaconid and the entoconid, and it is rather small. The hypoconulid shelf is worn. The m2 is oval shaped and is slightly broader mesially. Mesially, the metaconid is of similar height with the protoconid but the protoconid is larger. These two cusps are not set close to each other, having some space between them. The hypoconid is positioned distobuccally and is smaller than the other two cusps. Distolingually there is no entoconid on the cingulum. The cingulum is well-developed mesiobuccally. The m3 is missing.

3.3 *Canis* (*Xenocyon*) sp.

3.3.1 Material

Upper dentition: TSR-46, right M1.

3.3.2 Description

TSR-46 (Pl. III, Fig. 9) has a large and high paracone compared to the smaller metacone. These two cusps are set close together. The protocone is well-developed, tall and not so mesially placed. The metaconule is crista-like, not a clear cusp. The hypocone is bilobate and separated from the cingulum on the distolingual part. The lingual cingulum, even though developed, it is rather low. The buccal cingulum is very strong. The trigon basin is much more developed and deeper unlike the talon one.

3.4 Comparisons

3.4.1 Cranial and dental comparison with middle-sized canids of the European Early Pleistocene

Cranium

Both crania, TSR-D17-37a and TSR-G20-11a seem moderately elongated in dorsal view and the nasal bones end beyond the maxillofrontal suture at the TSR G20-11a (in TSR D17-37a the suture is not clearly visible, only estimated). In *Canis arnensis* the cranium is modestly elongated but the nasals are shorter, ending at, or slightly before the level of the maxillofrontal suture (Bartolini Lucenti and Rook, 2016). On the other hand, *Canis etruscus* displays a more elongated snout with elongated nasals, whose margins end well beyond the maxillofrontal suture, and the same condition occurs in *C. accitanus* (Garrido and Arribas, 2008; Bartolini Lucenti et al., 2017). *Canis mosbachensis* has also long nasals that end beyond the suture (Bartolini Lucenti et al., 2017). The palate of TSR-G20-11a is narrower compared to TSR-D17-37a. The outline of the nuchal crest of TSR-G20-11a is more blunt and slightly distally inclined, whereas in TSR-D17-37a tends to be more triangular and ventrally curved. *Canis etruscus* and *C. borjgali* have been described to have blunt outline of the nuchal crest, *C. arnensis* has rounded whereas *C. mosbachensis* has triangular (Bartolini Lucenti et al., 2020).

In ventral view, the tympanic bullae of TSR-G20-11a seem more inflated compared to the ones of TSR-D17-37a (Fig. 8). The medial walls of the tympanic bullae are divergent to each other, at least at TSR-D17-37a; in TSR-G20-11a the divergence is not clear due to deformation. Although the divergence occurs in TSR-D17-37a, it is not as distinct as in the case of *C. borjgali* and *C. mosbachensis* (Sotnikova and Rook, 2010; Bartolini Lucenti et al., 2017, 2020). *Canis etruscus* and *C. arnensis* on the other hand, both have parallel to each other medial walls of the tympanic bullae (Bartolini Lucenti et al., 2017). The basioccipital of TSR-D17-37a forms a sharp ridge in the middle, whereas in TSR-G20-11a this ridge is much smoother.

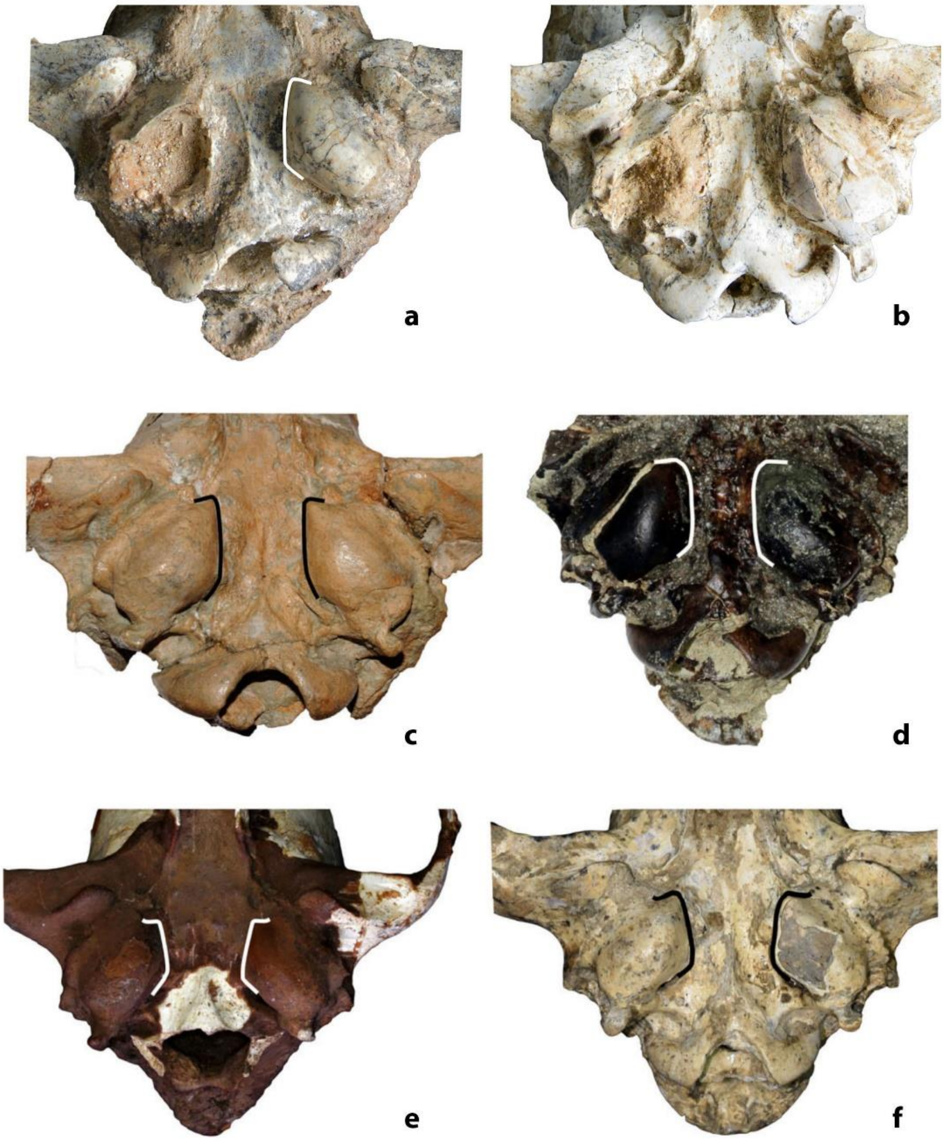

Figure 8. Comparison of the tympanic region in European *Canis*. **a**. TSR-D17-37a, *C. borjgali* vel *apolloniensis* from Tsiotra Vryssi; **b**. TSR-G20-11a, *C*anis sp. (morphotype B) from Tsiotra Vryssi; **c**. *C. etruscus* from Upper Valdarno; **d**. *C. arnensis* from Poggio Rosso; **e**. *C. mosbachensis* from Cueva Victoria; f. *C. borjgali* from Dmanisi. Pictures c–f taken from Bartolini Lucenti et al. (2020).

In ventral view, small diastemata can be found between the upper premolars of TSR-G20-11a, but not in TSR-D17-37a. Diastemata are present in *C. arnensis*, but they can also be found in *C. etruscus* and in *C. accitanus*. The presence of diastemata between the upper premolars is generally diverse, for example *C. mosbachensis* from Untermassfeld and *C. apolloniensis* display both absence and presence, thus this character is probably not of diagnostic significance (Sotnikova, 2001; Koufos et al., 2018).

Upper teeth

P3 and P4 clearly deviate from one another in TSR-D17-37a whereas in TSR-G20-11a the divergence is small; the teeth are almost inline. In *C. arnensis* and *C. etruscus* the axis of P3 is in line with that of P4, in *C. borjgali* the deviation may be present, but in *C. apolloniensis* and *C. mosbachensis* a deviation is generally observed (Bartolini Lucenti et al., 2020).

The P4 is slender on the TSR-G20-11a, and its protocone is small and not so mesially placed whereas in TSR-D17-37a it is better developed but still not large; it is also more lingually placed, similar to *C. apolloniensis*. The P4 protocone of *C. arnensis* is small and never extends beyond the mesial margin of the tooth (Bartolini Lucenti and Rook, 2016), but in *C. etruscus* it is well-developed and elevated. *Canis borjgali* possesses also a small protocone, whereas *C. mosbachensis* from Untermassfeld has a better developed one (Sotnikova, 2001; Koufos, 2018; Bartolini Lucenti et al., 2020). Although *C. apolloniensis* has a small and low protocone (Koufos, 2018) it is sharper, taller, and more mesiolingually placed compared to both TSR specimens. *Canis orcensis* has a small protocone, which is located close to the paracone (Martínez-Navarro et al., 2021). Additionally, the mesial preparacrista of the P4 is more pronounced on TSR-D17-37a than to TSR-G20-11a. *Canis apolloniensis* has mesially a similar preparacrista and a double protocone crista like in TSR-D17-37a.

In M1 (Fig. 9), TSR-G20-11a and TSR-D17-37a possess paracones that are larger than the metacones. *Canis arnensis* is the only species that its paracone is of similar size and slightly larger than the metacone (Bartolini Lucenti and Rook, 2016). However, this character does not seem to apply in every specimen. TSR-G20-11a clearly possesses a protoconule on the mesial part, that is missing from TSR-D17-17a. *Canis accitanus* shows a distinct protoconule close to the protocone (Garrido and Arribas, 2008). The M1 protoconule has not been observed in *C. orcensis* (Martínez-Navarro et al., 2021), whereas it can be present in the rest species. Probably the presence or absence of the protoconule is not a safe diagnostic character at the species level. The metaconule of TSR-G20-11a and TSR-D17-37a is a distinct cusp compared to *C. orcensis* and *C. accitanus* that display a crista-like metaconule in M1 (Garrido and Arribas, 2008; Martinez-Navarro et al., 2021). Regarding the trigon and talon basins, the medium-sized TSR canids have deeper trigon basins, unlike *C. etruscus* and *C. arnensis* whose M1 basins are of the same depth (Bartolini Lucenti et al., 2017). The large M1 specimen TSR-46 is comparable in size with *C. etruscus*, however does not share the same morphology, for example its talon and trigon basins are not of the same depth; the talon one is weakly developed. Compared to TSR-D17-37a and TSR-G20-11a, the M1 of TSR-46 is larger and has a crista- like metaconule. The trigon basin of TSR-46 is also more developed and its hypocone more distinct in contrast to the TSR medium- sized taxa. The distolingual margin of the M1 at the area of the hypocone, is more elevated in TSR-G20-11a than in TSR-D17-37a. TSR-D17-37a bears an additional cusp mesiolingually. *Canis apolloniensis* displays generally a lingual elongation on the M1 talon compared to the TSR ones.

The contact area between M1 and M2 is wider in TSR-G20-11a compared to TSR-D17-37a. This character best distinguishes *C. arnensis*, which is described as having a broad space between M1–M2, from *C. etruscus* that has a reduced one (Cherin et al., 2014). This contact area seems however variable; *C. orcensis* has a broad area, *C. accitanus* something in between and *C. apolloniensis* mostly reduced. Hence little diagnostic credibility may apply on this feature.

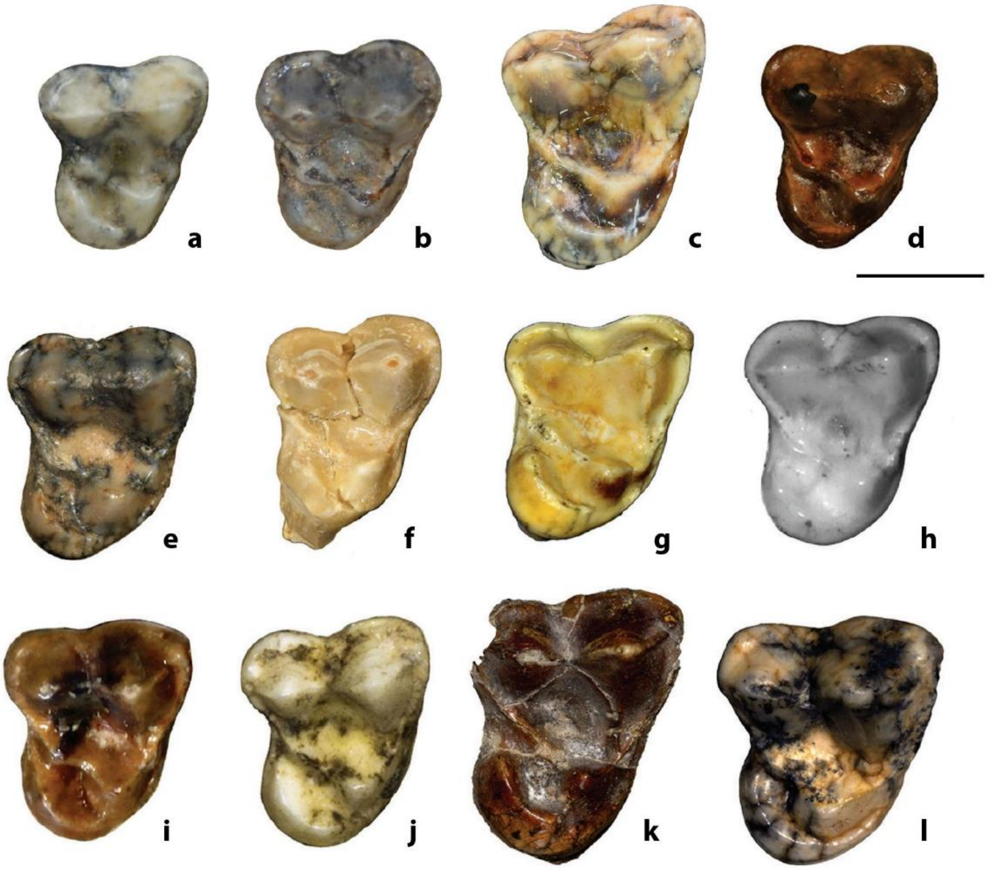

Figure 9. Comparison of right M1 of medium- and large-sized canids from various European localities. **a**. TSR-G20-11a, *Canis* sp. (morphotype B) from Tsiotra Vryssi (reversed); **b**. TSR-D17-37a, *C. borjgali* vel *apolloniensis* from Tsiotra Vryssi; **c**. TSR-46, *C.* (*Xenocyon*) sp., from Tsiotra Vryssi; **d**. IGF 869, *C. arnensis* from the Upper Valdarno; **e**. APL-16, *C. apolloniensis* from Apollonia-1; **f**. VM-2258, *C. orcensis* from Venta Micena; **g**. EVT-6530, *C. mosbachensis* from Vallparadís Section; **h**. FP1-2001-0434, *C. accitanus* from Fonelas P-1 (Garrido and Arribas 2008); **i**. IGF 12867, *C. etruscus* from Matassino (Upper Valdarno); **j**. D2314, *C. borjgali* from Dmanisi; **k**. IGF 883, *C.* (*X.*) *falconeri* from the Upper Valdarno; **l**. PP

186, *C.* (*X.*) *lycaonoides* from Pirro Nord. Scale bar: 1 cm. Pictures d–l taken from Martínez-Navarro et al. (2021).

The M2 of TSR-G20-11a is more buccolingually elongated and long compared to the TSR-D17-37a one, which is narrower and tends to be squared. However, they share same cusp morphology; the paracone is larger than the metacone and the protocone is well developed, in contrast to *C. arnensis* in which the two buccal cusps are equally sized (Bartolini Lucenti et al., 2020). Compared to *C. apolloniensis*, the medium-sized TSR canids share similar morphology, but the M2 of *C. apolloniensis* is larger buccolingually.

Mandible

The mandible TSR-G20-11b is slenderer compared to TSR-D17-37b and also displays a much shallower masseteric fossa. Compared to *C. apolloniensis*, they all share short mandibles that are rather thin, although TSR-D17-37b is more robust. The toothrow curvature (p1–m3 in line or the teeth between them deviate from one another) on the mandible is strong on the medium-sized canids of TSR and differs from that seen in *C. arnensis* that shows a rather straighter toothrow (Bartolini Lucenti and Rook, 2016). Some small diastemata occur in TSR-G20-11b whereas in TSR-D17-37b the premolars are set close to each other.

Lower teeth

Generally, the morphology of the lower teeth is similar on both TSR medium-sized canids. They both possess a distal cuspid on p3, but it is less developed in TSR-D17-37b. This cuspid is also reduced in *C. apolloniensis* and *C. mosbachensis* (Bartolini Lucenti et al., 2020). Compared to *C. etruscus* and *C. arnensis*, the p3 alveoli (Fig. 10) are set lower in the mandible between p2 and p4, especially distally, but not at the same level as in *C. borjgali*, or *C. mosbachensis* (Bartolini Lucenti et al., 2020).

The p4 of TSR-D17-37b is distally more inflated compared to TSR-G20-11b and its protoconid is more distally inclined than the latter one (Fig. 10). Their distal accessory cuspid is separated from the distal cingulid but it is very small. In *C. apolloniensis* this cuspid may be also separated (Koufos, 2018); in *C. orcencis* it is separated (Martínez-Navarro et al., 2021); in *C. mosbachensis* and *C. borjgali* it is fused with the distal cingulid (Bartolini Lucenti et al., 2020). The height of the protoconids of p4 is shorter or of similar height compared to the m1 paraconid, like in *C. orcensis* and *C. apolloniensis*.

On m1 (Fig. 10), the mesial margin of the paraconid of both TSR medium-sized canids, is distally inclined like in *C. apolloniensis*, *C. orcensis*, *C. borjgali* or *C. mosbachensis* and differs from the vertical figure that *C. etruscus* and *C. arnensis* display (Bartolini Lucenti et al., 2017). The m1 paraconid of *C. apolloniensis* also displays distal inclination, but in most specimens, it is rather tall, taller than in the TSR ones. The metaconid is well individualised from the protoconid in both TSR-G20-11b and TSR-D17-37b, but in *C. apolloniensis* some specimens have smaller metaconids.

Both TSR medium-sized canids also differ from *C. arnensis* in having a sinuous transverse crest that connects the hypoconid with the entoconid; this crest has been described as straight in *C. arnensis*. Additionally, their hypoconids are larger than the entoconids; in *C. arnensis* they are of similar size (Martínez-Navarro et al., 2009; Bartolini Lucenti et al., 2017). In *C. etruscus* the m1 hypoconid is described as very large and the transverse cristid can be both straight or sinuous (Bartolini Lucenti et al., 2017). TSR-D17-37b and TSR-G20-11b possess accessory cuspids (entoconulid) in the m1, between the metaconid and the entoconid on the distolingual side, as in *C. apolloniensis*, *C. borjgali*, *C. mosbachensis* and unlike *C. etruscus* (Bartolini Lucenti et al., 2020). Overall, the m1 morphology of the TSR medium-sized canids is more similar to that of the *C. mosbachensis* lineage than to *C. etruscus* or *C. arnensis* in *sensu stricto.*

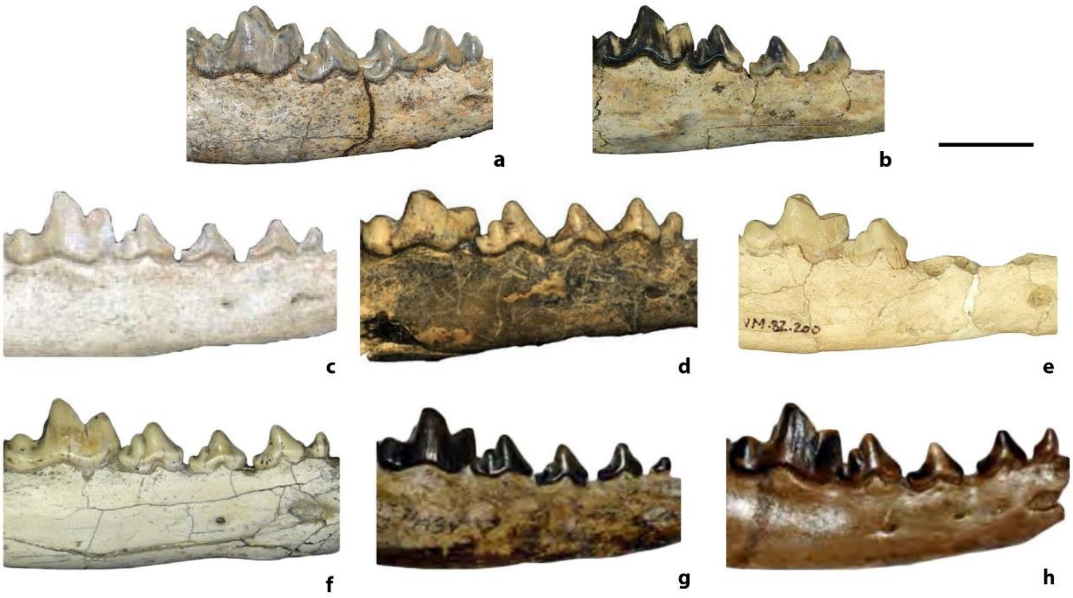

Figure 10. Buccal morphology of the p2–m1 of the right hemimandible of various European *Canis* species. **a**. TSR-D17-37b, *C. borjgali* vel *apolloniensis* from Tsiotra Vryssi (reversed); **b**. TSR-G20-11b, *Canis* sp. (morphotype B) from Tsiotra Vryssi; **c**. LGPUT-APL-530, *C. apolloniensis* from Apollonia-1 (reversed), taken from Koufos (2018); **d**. D4871, *C. borjgali* from Dmanisi, taken from Bartolini Lucenti et al. (2020); **e**. VM-2253, *C. orcensis* from Venta Micena, taken from Martinez-Navarro et al. (2021); **f**. EVT24342, *C. mosbachensis* from Vallparadís, taken from Bartolini Lucenti et al. (2017); **g**. IGF 7419V, *C. arnensis* from Poggio Rosso, taken from Bartolini Lucenti (2015); **h**. IGF 11800, *C. etruscus* from Upper Valdarno, taken from Bartolini Lucenti (2015). Scale bar: 2 cm.

Unlike *C. arnensis*, the TSR medium-sized canids have larger protoconids than metaconids on the m2 and there are no accessory cuspids found distolingually; they lack any entoconid and only the cingulum is developed (e.g., Bartolini Lucenti et al., 2020). This character separates *C. arnensis* from *C. mosbachensis* (Martínez-Navarro et al., 2009) as well *C. orcensis*, *C. borjgali* and *C. apolloniensis*. The two m2 mesial cuspids (protoconid and entoconid) are not so close situated to each other in TSR-G20-11b contra to TSR-D17-37b.

Selected craniodental characters of European *Canis* species that were previously discussed, are given in Table 2.

Table 2. Summarizing table of several craniodental features of *C. etruscus*, *C. arnensis*, *C. apolloniensis*, *C. mosbachensis*, *C. borjgali* and *C. orcensis* in comparison to the TSR *Canis* taxa: *C. borjgali* vel *apolloniensis* (TSR-D17-37) and *Canis* sp. (morphotype B) (TSR-G20-11). Modified table from Bartolini Lucenti et al. (2020); data for *C. orcensis* from Martínez-Navarro et al. (2021); data for *C. apolloniensis* are revised.

Character	*C. etruscus*	*C. arnensis*	*C. apolloniensis*	*C. mosbachensis*	*C. borjgali*	*C. orcencis*	TSR-G20-11	TSR-D17-37
Nasal bones/ maxillofrontal suture	very long, end well beyond	short, end slightly before	-	long, end beyond	long, end beyond	-	end beyond	end beyond
Outline of nuchal crest	blunt	rounded	-	triangular, sharp-pointed	blunt	-	blunt	blunt-triangular
Medial walls of the tympanic bullae	straight, parallel one another	straight, parallel one another	-	markedly rostrocaudally divergent	markedly rostrocaudally divergent	-	-	slightly rostrocaudally divergent
Axis of P3/P4	inline	inline	P3 generally deviates laterally	P3 generally deviates laterally	P3 may deviate laterally	-	inline	P3 deviates laterally
Trigon-talon basins on M1	same depth	same depth	trigon basin deeper	trigon basin deeper	trigon basin deeper	trigon basin deeper	trigon basin deeper	trigon basin deeper
M2 metacone	smaller than the paracone	equal-sized with paracone	similar to the paracone	smaller than the paracone	smaller than the paracone	smaller than the paracone	smaller than the paracone	smaller than the paracone
p3 distal accessory cuspulid	developed	developed	generally reduced	generally reduced	present	present	present	present
p3 alveolus/ level of p2-p4 alveoli	at same level	at same level	generally at same level	lower	lower	lower	lower	lower
p4 secondary distal cuspulid and distal cingulid	separated	separated	fused	fused	fused	separated	separated	separated
Mesial margin of paraconid of m1	vertical and straight	vertical and straight	inclined distally and straight/ slightly curved	inclined distally and straight/ slightly curved	inclined distally and straight	inclined distally	inclined distally/ curved	inclined distally/ curved
hypoconid of m1	very large	similar size with entoconid	considerably larger than the entoconid	larger than the entoconid	larger than the entoconid	larger than the entoconid	larger than the entoconid	larger than the entoconid
Transverse cristid of m1 talonid	straight (rarely sinuous)	straight	straight (rarely sinuous)	generally sinuous	generally sinuous	prominent sinuous	sinuous	sinuous
m1 accessory cuspids	absent	can be present	generally present	generally present	can be present	present	present	present
m2 protoconid	larger than the metaconid	equal-sized with metaconid	larger than the metaconid	larger than the metaconid	larger than the metaconid	larger than the metaconid	larger than the metaconid	larger than the metaconid
m2 distolingual cuspids	absent	entoconid evident	generally absent	generally absent	absent	absent	absent	absent

3.4.2 Dental comparison with large-sized canids of the European Early Pleistocene

The large M1 specimen from TSR is additionally compared to the large-sized canids from Europe. The general morphology of TSR-46 M1, fits the original description of *C*. (*X*.) *lycaonoides* from Gombasek (Slovakia; Kretzoi, 1938); it has a larger and higher paracone compared to the metacone, a well-developed protocone, and the metaconule is absent (crest-like). The trigon basin is well-developed, and the talon basin is reduced as in *Canis* (*Xenocyon*) (Martínez-Navarro and Rook, 2003). It resembles *C*. (*X*.) *falconeri* from Upper Valdarno and also the more derived *C*. (*X*.) *lycaonoides* (Fig. 9). It lacks any protoconule mesially as *C*. (*X*.) *falconeri* (Martínez-Navarro et al., 2021). The *C*. (*X*.) *lycaonoides* from Apollonia-1 is more triangular in shape and more robust, and its metaconule is not crest-like compared to the TSR one.

3.4.3 Metrical comparison of medium- and large-sized canids of the European Early Pleistocene

The proposed ratios of Cherin et al. (2014) are provided in Figures 11 and 12. The GLN/TL box plot (Fig. 11) reveals that *C. etruscus* is well separated from the rest of the *Canis* species, portraying remarkably long nasals. The TSR specimens on the other hand, are placed on the extremes of *C. borjgali* range. TSR-G20-11a is also found close to *C. accitanus* and the upper range of *C. arnensis*. The two TSR specimens are not very close to each other, but still within the range of *C. borjgali*.

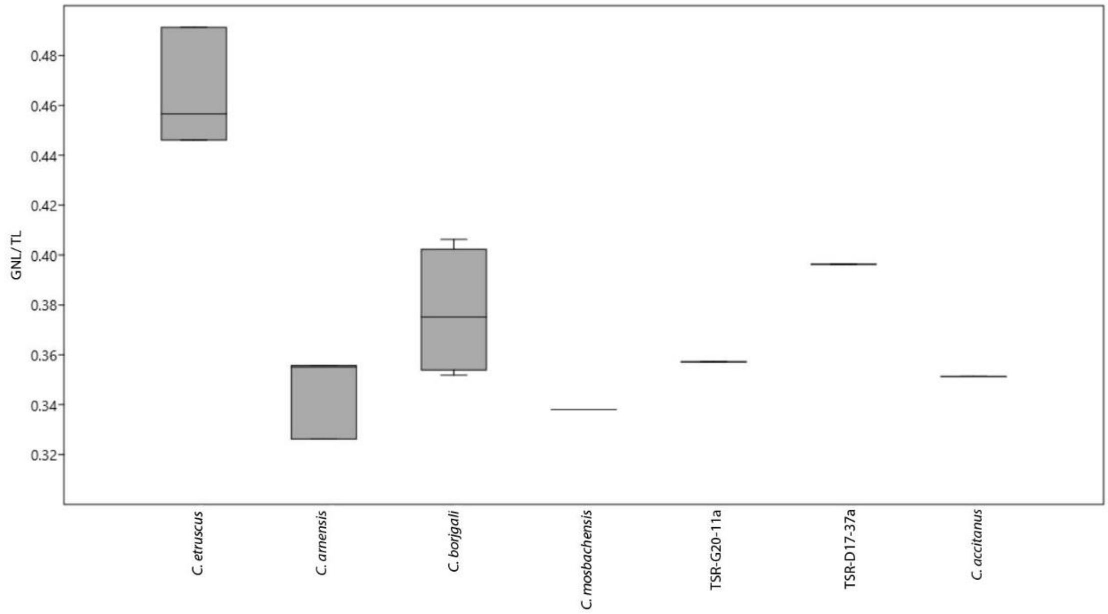

Figure 11. Box plot of the greatest length of the nasals/ total length of the cranium (GNL/ TL) ratio of European and TSR canids. *C. etruscus* from Olivola and Pantalla (*n* = 3); *C. arnensis* from Il Tasso and Poggio Rosso (*n* = 3); *C. borjgali* from Dmanisi (*n* = 4); *C. mosbachensis* from Cueva Victoria (*n* = 1); *C. accitanus* from Fonelas P-1 (*n* = 1); TSR-G20-11a, *Canis* sp. (morphotype B) and TSR-G17-37a, *C. borjgali* vel *apolloniensis* from Tsiotra Vryssi.

The LMR/LCR ratio seems to clearly separate *C. arnensis* from the rest canids, although *C. etruscus* displays a wide range of proportions (Fig. 12). TSR-D17-37a is placed within the range of all canids, except for *C. arnensis*, whereas TSR-G20-11a shows a certainly lower ratio in between those of *C. etruscus* and *C. arnensis*.

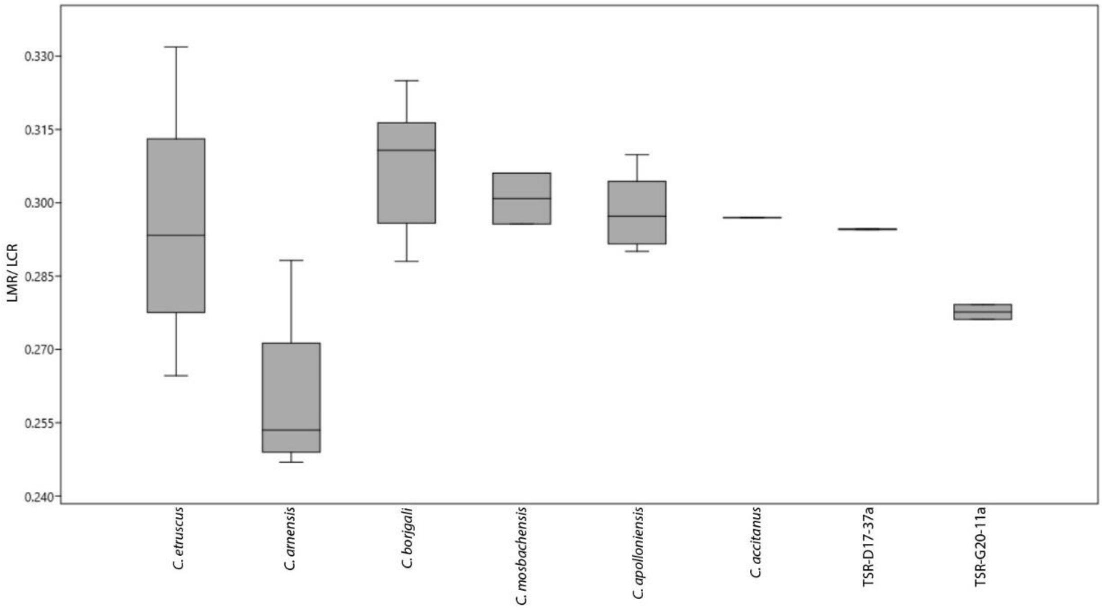

Figure 12. Box plot of the upper molar row/ cheektooth row length (LMR/ LCR) ratio box plot of European and TSR canids. *C. etruscus* from Italy (*n* = 5); *C. arnensis* from Il Tasso and Poggio Rosso (*n* = 5); *C. borjgali* from Dmanisi (*n* =14); *C. mosbachensis* from Cueva Victoria (*n* = 2); *C. apolloniensis* from Apollonia-1 (*n* = 5); *C. accitanus* from Fonelas P-1; TSR-D17-37a, *C. borjgali* vel *apolloniensis* (*n* = 2) and TSR-G20-11a, *Canis* sp. (morphotype B) (*n* = 2) from Tsiotra Vryssi.

The M1 length/ width scatter plot (Fig. 13) shows that the large M1 specimen from TSR (TSR-46) is very close to the dimensions of the lectotype of *C. etruscus* (MPM 47) from Upper Valdarno (which marks the uppermost range of this species), however it is not plotted far from the range of *C.* (*X.*) *lycaonoides*. The rest of the taxa are greatly overlapping, but the smaller TSR canid is plotted close to *C. accitanus*, yet both are within lower limits of *C. mosbachensis* range. TSR-G16-46 is also within the area of overlap between *C. mosbachensis* and *C. arnensis*. Moreover, it is of intermediate size between TSR-G20-11a and TSR-D17-37a. All medium-sized specimens are found within the wide range of *C. mosbachensis* and are clearly separated from the large-sized specimen (TSR-46).

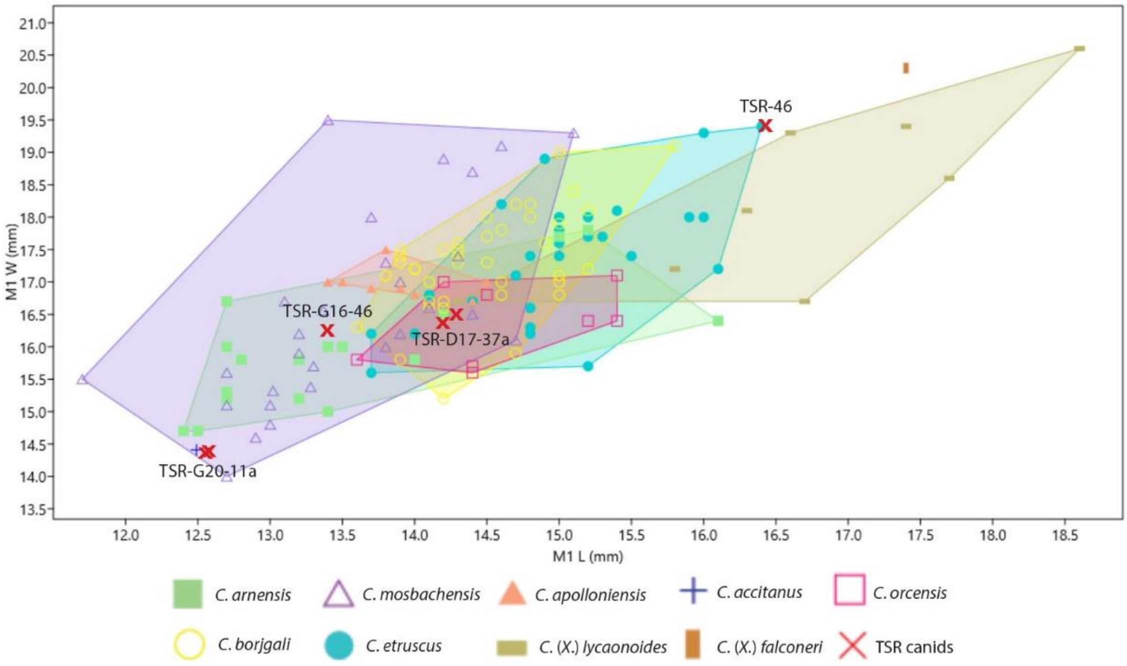

Figure 13. Scatter plot of length/ width of M1 of TSR canids in comparison to several European ones. *C. arnensis* from Italy; *C. etruscus* from Italy; *C. borjgali* from Dmanisi; *C. mosbachensis* from Untermassfeld, Pirro Nord and Vallparadís; *C. apolloniensis* from Apollonia-1; *C. orcensis* from Venta Micena; *C. accitanus* from Fonelas P-1; *C.* (*X.*) *lycaonoides* from Apollonia-1, Pirro Nord and Gombasek*;* C. (*X.*) *falconeri* from Upper Valdarno; TSR-G20-11a, *Canis* sp. (morphotype B), TSR-D17-37a; TSR-G16-46, *C. borjgali* vel *apolloniensis* and TSR-46, *Canis* (*Xenocyon*) sp. from Tsiotra Vryssi.

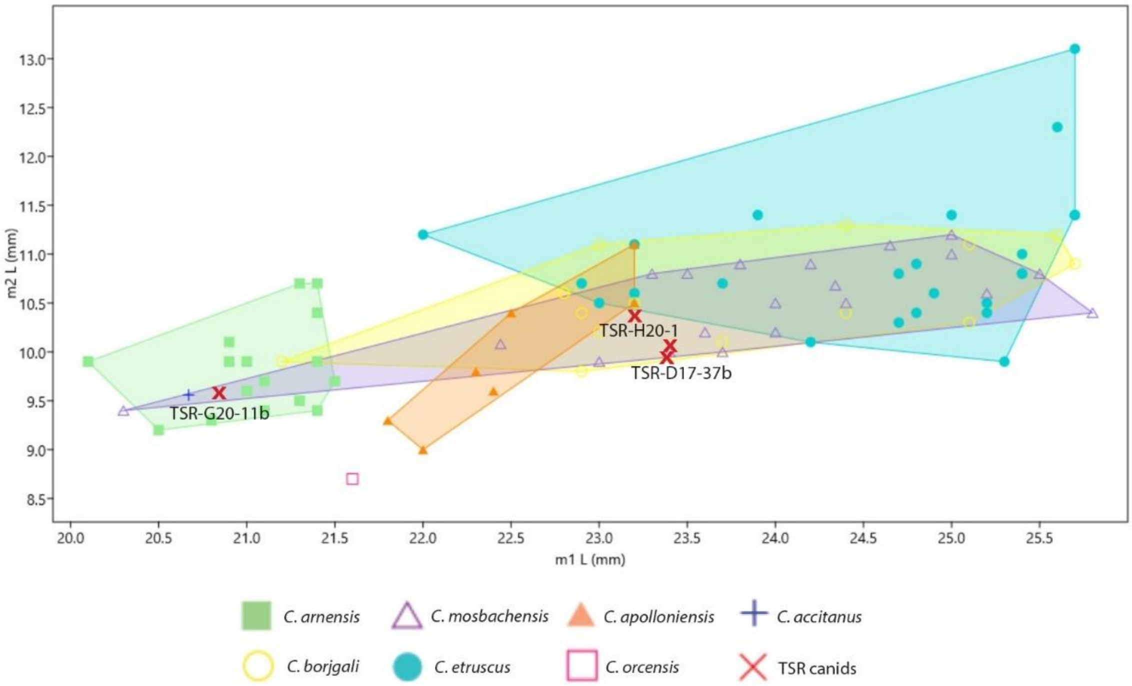

Figure 14. Scatter plot of m1/ m2 length, of European and TSR canids. *C. arnensis* from Italy; *C. etruscus* from Italy; *C. borjgali* from Dmanisi; *C. mosbachensis* from Untermassfeld, Pirro Nord and Vallparadís; *C. apolloniensis* from Apollonia-1; *C. orcensis* from Venta Micena; *C.*

accitanus from Fonelas P-1; TSR-G20-11b, *Canis* sp. (morphotype B) and TSR-D17-37b; TSR-H20-1, *C. borjgali* vel *apolloniensis* from Tsiotra Vryssi.

The diagram of m1 length/m2 length ratio (Fig. 14) clearly separates *C. arnensis* from *C. etruscus*. The three TSR specimens are plotted within the range of *C. mosbachensis* and *C. borjgali* and are also very close to *C. apolloniensis*. TSR-G20-11b along with *C. accitanus* are closer to *C. arnensis* proportions, but still within the range of *C. mosbachensis*. The variability of *C. mosbachensis* in the given proportions seems rather wide.

Regarding the Simpson's log ratio diagram of the upper dentition (Fig. 15), it is clear that the smaller TSR canid (TSR-G20-11a) is of similar size and proportions with *C. accitanus*, especially at the last premolar and the two molars. On the contrary the TSR-D17-37b is placed within the group of the other canids (*C. etruscus*, *C. apolloniensis*, *C. orcensis*, *C. borjgali*) but seems to portray some unique proportions such as the large width of the P1 and the small length of the M2. On the lower teeth (Fig. 16), again, TSR-G20-11b is found closer to the incomplete proportions of *C. accitanus* and seems to have a long talonid on the m1. TSR-D17-37b is placed closer to *C. etruscus* and *C. borjgali*.

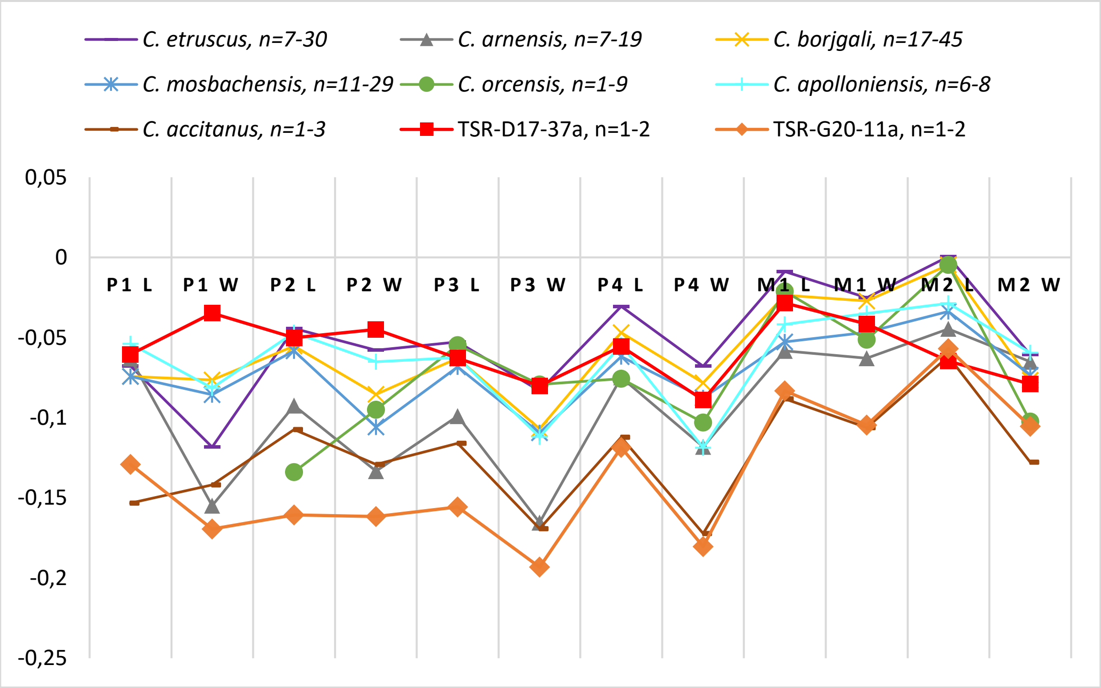

Figure 15. Simpson's log ratio diagram for the upper dentition, P1–M2 comparing the TSR canids to several European ones. *C. etruscus* from Italy; *C. arnensis* from Italy; *C. borjgali* from Dmanisi; *C. mosbachensis* from Untermassfeld, Pirro Nord, Vallparadís, Cueva Victoria; *C. orcensis* from Venta Micena; *C. apolloniensis* from Apollonia-1; *C. accitanus*; TSR-G20-11a, *Canis* sp. (morphotype B) and TSR-D17-37a, *C. borjgali* vel *apolloniensis* from Tsiotra Vryssi. Standard of comparison: mean values of *C. lupus italicus* (*n* = 209–253) from Sardella et al. (2014).

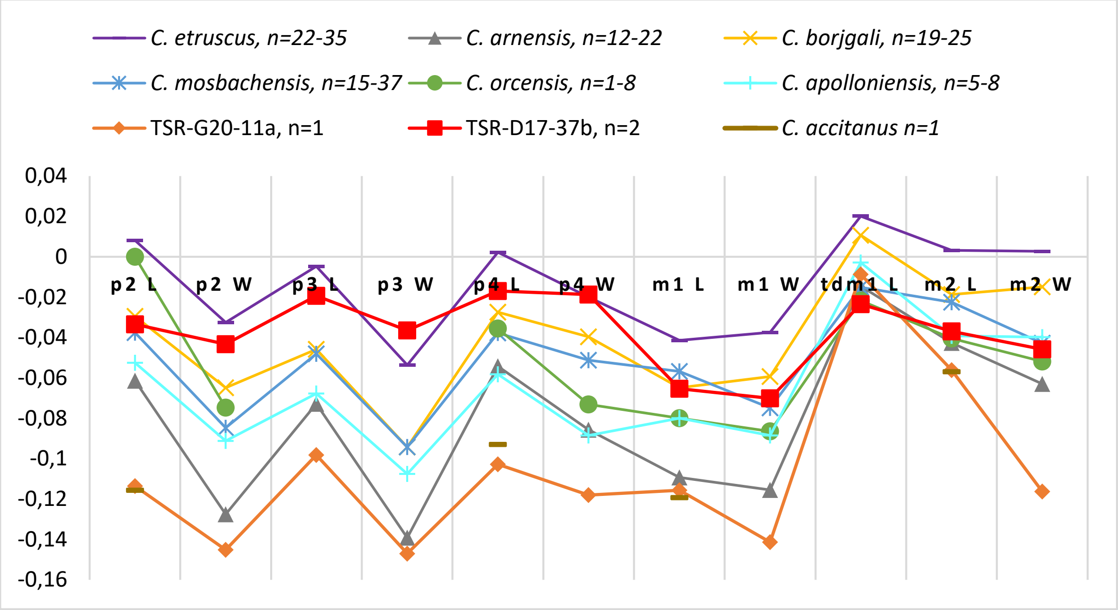

Figure 16. Simpson's log ratio diagram for the lower dentition, p2–m2 comparing the TSR canids to several European ones. *C. etruscus* from Italy; *C. arnensis* from Italy; *C. borjgali* from Dmanisi; *C. mosbachensis* from Untermaßfeld, Pirro Nord, Vallparadís, Cueva Victoria; *C. orcensis* from Venta Micena; *C. apolloniensis* from Apollonia-1; *C. accitanus*; TSR-G20-11a, *Canis* sp. (morphotype B) and TSR-D17-37b, *C. borjgali* vel *apolloniensis* from Tsiotra Vryssi. Standard of comparison: mean values of *C. lupus italicus* (*n* = 198–254) from Sardella et al. (2014).

The PCA of the upper toothrow dimensions (Fig. 17a) displays an overlapping of the species, leaving however outside *C. accitanus* and TSR-G20-11a. Additionally, *C. arnensis* partly differentiates from the rest of the overlapping species. TSR-D17-37b is within the ranges of *C. borjgali* and *C. mosbachensis* and not far from the maxima of *C. etruscus* and *C. apolloniensis*. The log-transformed upper teeth data (Fig. 17b) indicate that shape differences among upper dentitions of the several *Canis* species are less important; TSR-G20-11a is plotted within the overlapping convex hulls of *C. apolloniensis* and *C. etruscus*, whereas TSR-D17-37b is within *C. mosbachensis* variability and very close to *C. borjgali*.

The PCA of the lower teeth dimensions (Fig. 18a) shows a clearer separation of *C. arnensis* from the rest taxa (data for *C. accitanus* are missing). TSR-G20-11b appears closer to *C. arnensis*, clearly outgrouped from TSR-D17-37a which is placed within *C. borjgali* and *C. etruscus* ranges. As for the log-transformed data of the lower toothrow (Fig. 18b), they indicate not important shape differences among the various compared species; TSR-D17-37b sets outside the *C. etruscus* and *C. arnensis* range and closer to *C. orcensis*. TSR-G20-11b is grouped with *C. mosbachensis*.

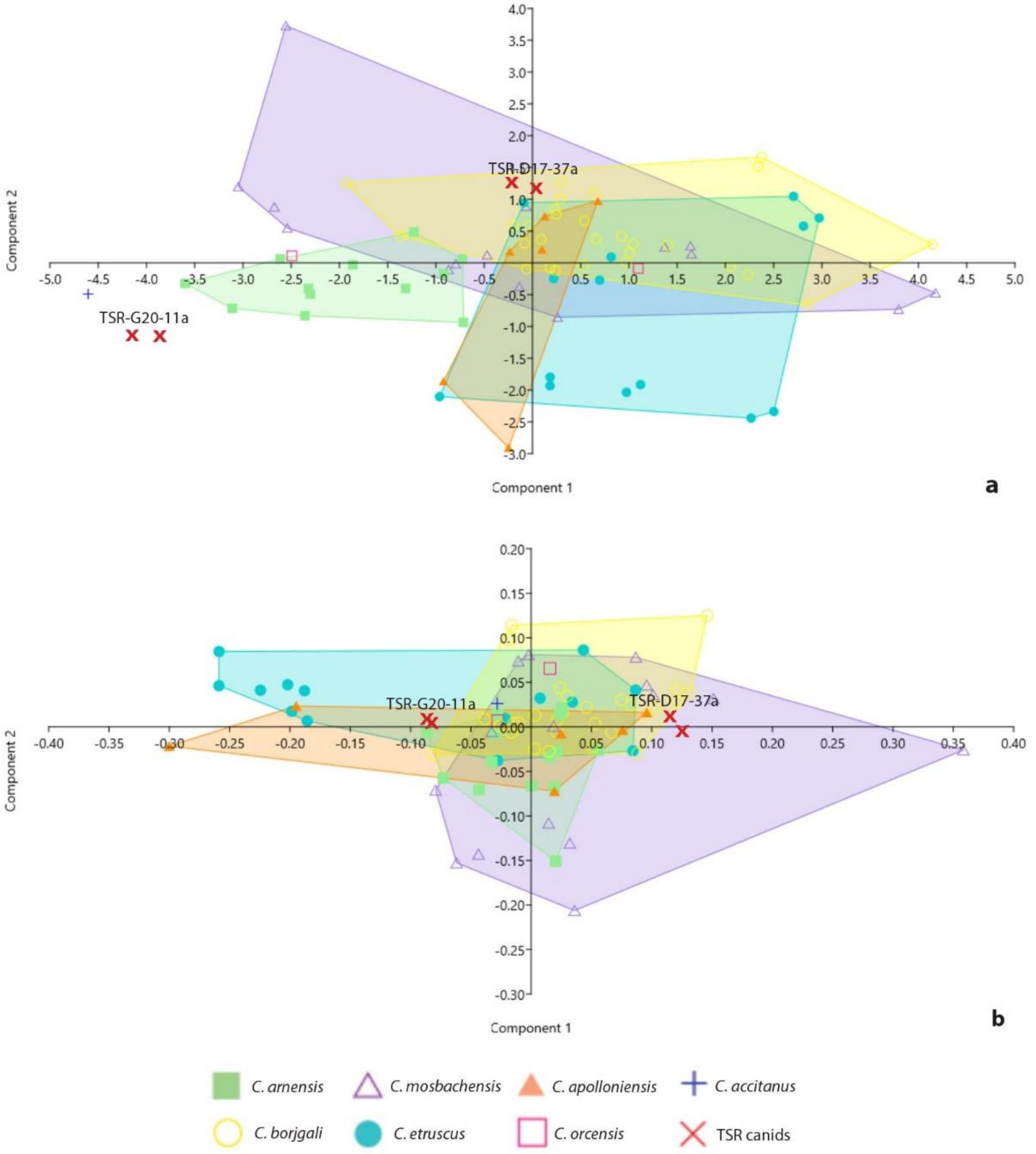

Figure 17. Principal component analysis (PCA) on **a.** upper teeth measurements (length and width of P4, M1, M2; only complete P4–M2 tooth rows are included). Variance (%): PC1-59.1 and PC2-18.5; **b.** log-transformed measurements. Variance (%): PC1-59.5 and PC2-18.9. *C. arnensis* from Italy; *C. etruscus* from Italy; *C. borjgali* from Dmanisi; *C. mosbachensis* from Pirro Nord, Vallparadís, Cueva Victoria; *C. mosbachensis* from Untermassfeld, *C. apolloniensis* from Apollonia-1; *C. orcensis* from Venta Micena; *C. accitanus* from Fonelas P-1; TSR-G20-11a, *Canis* sp. (morphotype B) and TSR-D17-37a, *C. borjgali* vel *apolloniensis* from Tsiotra Vryssi.

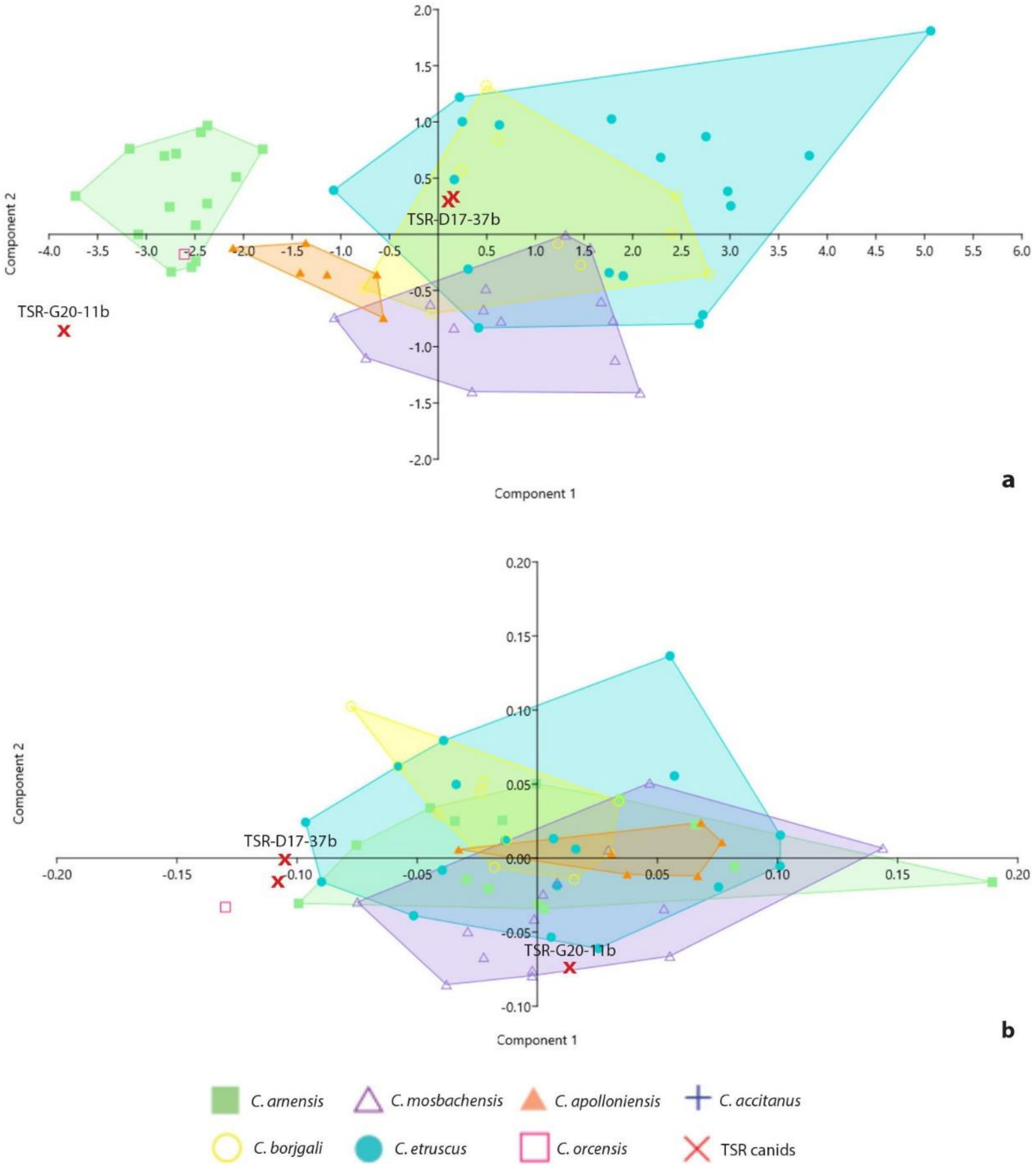

Figure 18. Principal component analysis (PCA) on **a**. lower teeth measurements (length and width of p4, m1, m2; only complete p4–m2 tooth rows are included). Variance (%): PC1-80.2 and PC2-9.4; **b**. log-transformed measurements. Variance (%): PC1-41.9 and PC2-21.5. *C. arnensis* from Italy; *C. etruscus* from Italy; *C. borjgali* from Dmanisi; *C. mosbachensis* from Pirro Nord, Vallparadís, Untermassfeld; *C. apolloniensis* from Apollonia-1; *C. orcensis* from Venta Micena; TSR-G20-11b, *Canis* sp. (morphotype B) and TSR-D17-37b, *C. borjgali* vel *apolloniensis* from Tsiotra Vryssi.

3.5 *Canis* sp. (postcranial skeleton)

3.5.1 Material

Postcranial skeleton (Pls. IV–VI).

- Axis articulated to the third cervical vertebra (TSR-G17-30)
- Fragmented sacrum (broken in half) (TSR-G18-41)
- Right scapula lacking proximal part (TSR-H18-22)
- Distal part of right scapula, right humerus with fragmented proximal epiphysis, left fragmented metacarpal bones (1–5), left proximal phalanges (2–5), left middle phalanges (2–3), left distal phalanges ($n = 2$) and sesamoid bones ($n = 2$) (TSR-G20-10a–g) of the same individual
- Fragmented right humerus with fragmented distal epiphysis, diaphysis with part of distal epiphysis of left humerus, proximal part with diaphysis of left ulna, fragmented proximal epiphysis with part of diaphysis of right radius, fragmented left radius (TSR-D18-90, 91, 91, 92, 93) of the same individual
- Right humerus (TSR-H18-27)
- Proximal epiphysis, part of diaphysis and distal epiphysis of left humerus (TSR-H18-15)
- Fragmented left humerus, lacking part of the distal epiphysis (TSR-H22-12)
- Proximal half of fragmented left ulna, distal half of fragmented left radius (TSR-H22-8a, 8b), of the same individual
- Right ulna, lacking the distal part (TSR-G20-44)
- Right radius (TSR-G21-86)
- Part of right hemipelvis (TSR-F16-28)
- Lumbar vertebrae ($n = 2\text{-}3$), sacrum, caudal vertebrae ($n = 10\text{-}11$), fragmented pelvis, part of proximal epiphysis and part of diaphysis of right femur, fragmented right tibia lacking part of the diaphysis, attached with fibula distally, distal part and part of diaphysis of left tibia, right calcaneus, left calcaneus, left astragalus with broken trochlea, right fragmented astragalus, right scaphoid, right cuboid, right cuneiforms, left cuboid, left cuneiform, right metatarsal bones (2–5), right proximal phalanges (2–5), right middle phalanges (2–5), right distal phalanges (2–5), left metatarsals lacking the distal epiphysis and part of diaphysis (2–4), left fifth metatarsal bone (5) (TSR-C17-18), of the same individual.
- Left fourth metatarsals lacking the distal part (4) (TSR-F21-7)
- Left fifth metatarsals lacking the distal part (5) (TSR-F20-44)
- Right third metacarpals (3) (TSR-G20-32)
- Right second metacarpals lacking the proximal part (TSR-F14-11)
- Fragmented left first metacarpal (1) (TSR-H21-5)
- Proximal phalanges (2–5), middle phalanges (3, 4, 5) (TSR-H22-10) of the same individual
- Unidentified proximal phalanges (TSR-G21-76, TSR-G20-38, TSR-C17-44, TSR-F16-31, TSR-G16-9)

- Unidentified middle phalanges (TSR-E21-60, TSR-F14-8, TSR-48b, TSR-F15-6)
- Unidentified distal phalanges (TSR-C17-17)

3.5.2 Description

Axis: It is represented by a single specimen that is articulated to a third cervical (C3). It has an elongated bladelike spinous process that extends cranially close to the level of the odontoid process (dens). The dens is thin and cylindrical extending cranially. The cranial articular surfaces (prezygapophysis) are small and rounded. The transverse processes of the axis are pointy and extend caudally on both sides. The caudal articular surfaces (postzygapophysis) are connected to the C3.

Sacrum: The anterior part is wide, where the wings extend on the sides. The cranial articular surfaces are large and are facing dorsomedially. Three large spinous processes extend dorsally, and two much smaller projections (mammillo- articular processes) occur laterally, on both sides accompanied by the dorsal sacral foramina. The body of the sacrum is dorsoventrally compressed. The caudal articular processes are small and posteriorly placed.

Caudal Vertebrae: The caudal vertebrae belong to the same individual. They all display the same processes; the cranial articular processes at the anterior, the caudal articular surfaces at the posterior and two transverse processes that extend posterolateraly. The first caudal vertebrae are wide with strong processes that tend to get thinner, smaller and simpler (more cylindrical) as they increase in number posteriorly.

Scapula: The scapula is represented by two specimens both having mainly the distal part preserved. On lateral view, the acromion processes are broken on both specimens and so is their dorsal extension, the spine which divides the scapula on the supraspinous fossa (anterior) and the infraspinous fossa (posterior). The preserved part of the anterior border is rounded whereas the posterior border is straight. The anterior border is concave at the distal part (scapular notch) reaching the supraglenoid tuberosity. The supraglenoid tuberosity is rounded and inflated anteriorly, and extends mesiodistally to the small, beaklike coracoid process. At the posterior part, the infraglenoid tuberosity is moderately developed. The glenoid cavity is shallow, subrounded and extends to the scapular tuberosity, which is hooklike.

Humerus: The material is represented by six specimens in total. At the proximal part, the head is oval shaped and strong extending to a beaklike end on the posterior. The greater tuberosity is laterally placed and is the highest elevation proximally forming a convex summit. The lesser tuberosity is located medially, as a flattened surface, that does not extend proximally to the level of the greater tuberosity. In anterior view, the intertubercular groove between these two tuberosities, is prominent. In lateral view, the head extends to the anconeal crest at the diaphysis and the anterolateral surface is rather smooth and wide. The diaphysis is long, cylindrical, and slightly sigmoid- shaped. On the distal epiphysis, a large supratrochlear foramen is present, visible on anterior and posterior view. The olecranon fossa is deep on the posterior. On anterior, the trochlea is prominent and along with the rounded capitulum at the lateral part, they are slightly laterally inclined. The medial epicondyle forms a prominent crest and it is larger than the lateral one. The lateral epicondyle is not very prominent and the lateral epicondyloid crest ends in a thick rounded form distally, on posterior view. In contrast, the distal end of the humerus, at the medial epicondyle, is strong and straight on the posterior.

Radius: Four specimens are known from TSR, but only one is completely preserved. The diaphysis is long, slender, slightly curved and anteroposteriorly flattened. The radial tuberosity is prominent medially, distal to the neck of the radius. The articular surface of the proximal epiphysis is smooth, unevenly oval-shaped. It is convex posteriorly and concave anteriorly. The distal epiphysis is wider compared to the proximal one. The distal articular surface is irregularly quadrilateral and slightly concave posterolaterally. The ulnar notch is a small, convex articular surface found at the lateral part. The styloid process is medially placed, extending to a sharp projection distally.

Ulna: The ulna is represented by three specimens. The olecranon process is found at the proximal epiphysis of the bone and is laterally compressed and medially inclined. On anterior view two small vertical projections are notable proximally on the olecranon; the medial one is taller. On medial view the proximal end of the olecranon is rounded posteriorly. The trochlear notch is vertically developed between the anconeal process and the coronoid process, it is a crescent- like, thin concavity. The anconeal process extends anteriorly and is medially inclined. The coronoid process distal of the trochlear notch, displays two projections laterally and medially. Between these two the radial notch is developed laterally facing. The bone gets thinner and cylindrical while reaching the distal part, which is not preserved in any of the specimens.

Metacarpals: The five preserved metacarpals are slender and elongated. The first metacarpal is flattened and very short. In dorsal view, the third and the fourth metacarpals are straight, and they are the longest ones, having a more triangular shape proximally. The second and the fifth metacarpals are both shorter and thicker, a bit inclined and four sided towards the proximal end. All metacarpals bear a condyle on the distal epiphysis. In ventral view the sagittal crest of the distal end is prominent. The proximal ends are irregular. The two palmar sesamoid bones that have been preserved are crescent- like.

Phalanges: The phalanges of the forepaw are very similar to the ones of the hindpaw, so the description includes both; the identification of the isolated specimens was hard to accomplish. The phalanges consist of three types, the proximal, the middle and the distal ones. The proximal epiphysis of the proximal phalange is wider than the distal one. Its articular surface forms a U-shaped concavity with two palmar tubercles connected with a deep groove. The distal epiphysis is saddle- shaped and two small condyles are visible. The third and fourth phalanges are straight on ventral view, and they are the longest. The second and the fifth ones, are both slightly medially curved. The middle phalanges are shorter and compressed towards the distal part. The proximal epiphysis has a sagittal ridge in the middle and small palmar tubercles. The distal epiphysis resembles the equivalent one of the proximal phalanges. The third and fourth middle phalanges are the longest. The distal phalanges possess a shallow concave articular surface, oval shaped, proximally. The distal part is laterally compressed and claw-like.

Pelvis: The complete pelvis is accompanied by lumbar and caudal vertebrae. It has typical canid morphology.

Femur: It is represented by a single specimen. Only the diaphysis is preserved and the greater trochanter at the proximal epiphysis. The diaphysis is long and slightly curved. The greater trochanter is laterally placed, pyramid-shaped and extends proximally. Posteriorly, the trochanteric fossa is deep, located between the greater trochanter and the missing head of the femur. The intertrochanteric crest is a wide arc shaped crest that runs the greater trochanter medially.

Tibia: The two preserved tibiae belong to a single individual. The proximal part is triangular, whereas the distal one is cylindrical. The proximal articular surface is triangular, including the lateral and medial condyles. The lateral condyle is oval shaped and concave transversely. It is cut out by a small, muscular notch, visible laterally. At the posterior view, between the two condyles, lays the popliteal notch. The tibial tuberosity viewed laterally, is a large proximally extended process, which distally prolongs to the tibial crest being slightly medially inclined. The lateral surface is smooth and wide, defined by the tibial crest. The medial surface is also smooth wide and flatter than the lateral one. The distal part of the bone is difficult to describe due to extensive deformity (pathology). Its lateral surface seems articulated to the distal part of the fibula. Medially, the medial malleolus is a distally extended process. The distal articular surface, although deformed, displays two inclined arc shaped grooves, the cochlea tibiae, separated by a ridge.

Astragalus: A single specimen is best-preserved. The proximal part is wide and larger than the distal one. The neck that connects these two uneven parts, is smooth and concave. The trochlea at the proximal part is broken. On plantar view, the middle articular surface is oval shaped. The distal part is small, rounded and irregularly oval shaped.

Calcaneus: The two calcanei specimens belong to the same individual. The proximal part (calcaneal tuber) is a strong elongated process, that extends to the lateral and medial processes. These two processes are joined by a wide groove. The distal part of the calcaneus is wider medially and has more complex morphology. Anteriorly, there are two/three smooth articular facets, one of them medially placed.

Metatarsals: The metatarsals mostly resemble in form the metacarpals, but they are longer. The major difference occurs at the morphology of the proximal articular surfaces, which are irregular but slightly more anteroposteriorly elongated.

The hindlimbs are generally represented by remains that belong to the same individual, except for the isolated metatarsals and phalanges. This particular individual, displays some pathological condition on its right hindlimbs, at the area of the junction of the tibia with the calcaneus and astragalus. Slight dysmorphia is also present in the left astragalus and calcaneus (Pl. IV).

3.5.3 Comparison in the postcranial skeleton

The description of the postcranial skeleton is on preliminary stage due to lack of identified comparative material from the rest localities of the Mygdonia basin, and the relatively poor literature on Plio-Pliostocene *Canis* postcranials. Measurements of Bonifay (1971), Sotnikova (2001) and Petrucci et al. (2013) were used for metrical comparison and additional images were studied from Torre (1967), Sotnikova (2001) and Petrucci et al. (2013).

The metrical comparison shows that the TSR postcranial elements are within the range or in cases slightly smaller than the dimensions provided by Bonifay (1971), Sotnikova (2001) and Petrucci et al. (2013) for European medium-sized canids (Tab. 3). Moreover, they are smaller than the known *Canis* (*Xenocyon*) postcranial remains from Untermassfeld and Pirro Nord (Tab. 4). Morphologically, the TSR remains in general resemble *C. mosbachensis* from Untermasseld, especially the smaller specimens.

Table 3. Greatest length of several skeletal parts of TSR and *C. mosbachensis* from Untermassfeld and L’ Escale given in mm. Modified table from Sotnikova (2001), data from Bonifay (1971) and Sotnikova (2001).

GL	Untermassfeld		L' Escale		Tsiotra Vryssi	
	n	range	*n*	range	*n*	range
Humerus	1	169	4	145–160	2	153.8–155.7
Radius	4	163–169	6	148–168	2	142.9–147.0
Tibia	4	181–191	7	160–191	1	~ 172.1
Astragalus	4	25.5–28.5	2	26–38.7	1	~ 24.1
Calcaneus	4	41.6- 47.5	2	24.4–39.2	2	41.1–42.2
Third Metacarpal	1	72.5	2	63.8–64.8	2	61.42–62.2
Third Metatarsal	3	73.9–81.1	2	71.4–72.5	1	70.5

Table 4. Greatest width of the distal end of the humerus from TSR, *C. mosbachensis* and *C.* (*X.*) *lycaonoides* from Untermassfeld and Pirro Nord, given in mm. Data from Sotnikova (2001) and Petrucci et al. (2013).

	C. mosbachensis		*C.* (*X.*) *lycaonoides*		*Canis* sp.
	Untermassfeld	Pirro Nord	Untermassfeld	Pirro Nord	Tsiotra Vryssi
WD	30.7	27.02	49.1	39.91	20.1 (min)– 26.74 (max)

In the studied postcranial remains from TSR, some size variance has been observed. It is not clear if it is the result of the presence of two *Canis* species, or due to intraspecific variation/sexual dimorphism. However, in some postcranial elements, such as the scapula, the humerus and the radius, additional morphological differences do occur.

In the case of the scapulae, TSR-H18-22 is larger compared to TSR-G20-10a. The infraglenoid tubercle is more pronounced on the smaller specimen. The surface of the glenoid cavity seems a little deeper in the smaller specimen whereas its outline is prominent on the larger specimen. The supraglenoid tubercle is moderately inflated in the smaller specimen (Fig. 19).

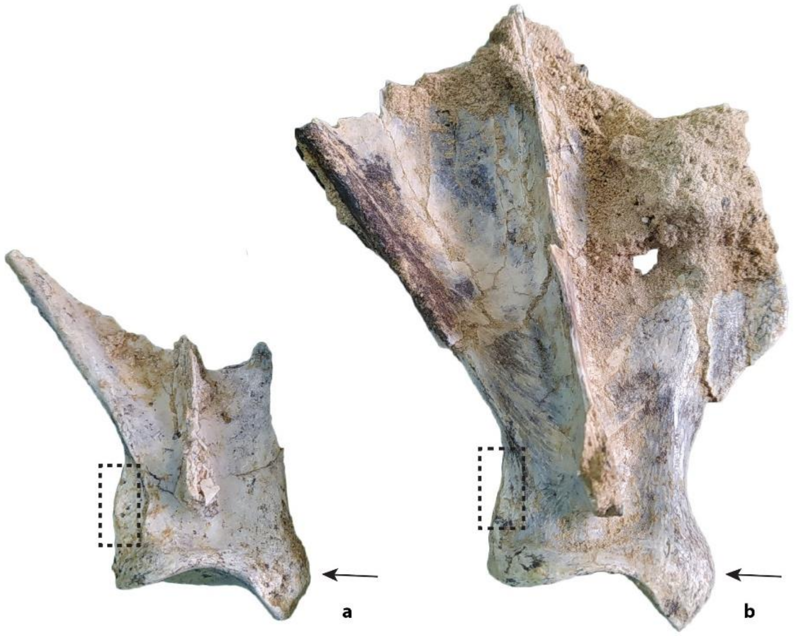

Figure 19. Comparison of two scapulae specimens from TSR. **a**. Right scapula, lateral view (TSR-G20-10a); **b**. Right scapula, lateral view (TSR-H18-22). The rectangle indicates the infraglenoid tuberosity area, the arrow indicates the supraglenoid tuberosity.

Four out of the six humeri are of the same size. The other two, TSR-G20-10 and TSR-H18-15 are slightly smaller (TSR-H18-15 is intermediate) and present some morphological alterations especially at the distal epiphysis (Fig. 20). The larger specimens are generally more robust compared to the smaller ones. The supratrochlear foramen seems wider in the smaller specimens. In posterior view, the medial epicondyle is much thinner in the smaller specimens, compared to the stronger ones of the larger individuals. In medial view, the small crest of the medial epicondyle is straight and thinner on the smaller specimens whereas in the larger specimens it is thicker and arched. Additionally, the distal end of the medial epicondyle is more proximally inclined on the larger specimens than to the smaller ones.

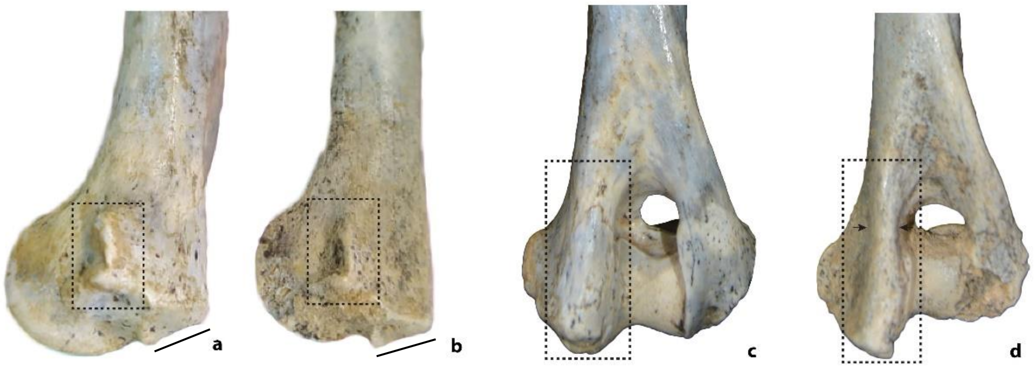

Figure 20. Comparison of the distal extremity of the two right humeri from TSR. **a**. TSR-H18-27, medial view; **b**. TSR-G20-10b, medial view; **c**. TSR-H18-27, posterior view; **d**. TSR-G20-10b, posterior view. The rectangle on a, b indicates the crest of the medial epicondyle, the rectangle on c, d indicates the posterior surface of the medial epicondyle, the line on a, b indicates the inclination of the distal end of the medial epicondyle.

Regarding the radii, only two are well preserved enough to be compared in detail. TSR-G21-86 is shorter than TSR-D18-92. The articular surface of the proximal epiphysis, which is preserved in both specimens, is smaller in TSR-G21-86 and simpler in outline compared to the more pronounced concave outline in TSR-D18-92 (Fig. 21).

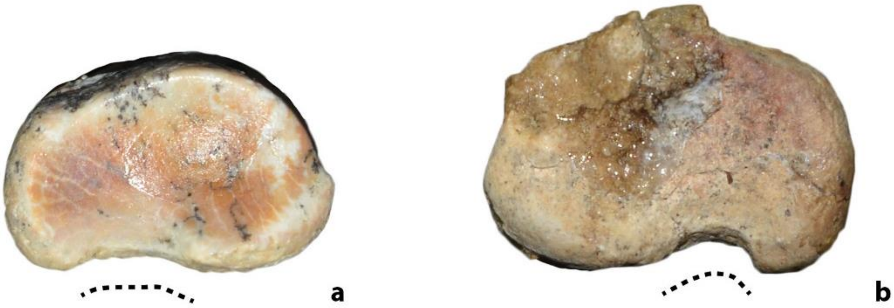

Figure 21. Comparison of the proximal articular surface of the two radii from TSR. **a**. Right radius, proximal view (TSR-G21-86); **b**. Left radius, proximal view (TSR-D18-92). The dashed line indicates the outline of the anterior border.

4. Discussion

The taxonomy of the Early Pleistocene European canids is generally debated. The newly discovered species *C. borjgali* from Dmanisi (Bartolini Lucenti et al., 2020) indicates an early differentiation of the *C. mosbachensis* lineage from the older and more basal *C. etruscus* and *C. arnensis*. The Dmanisi taxon changes the previous hypothesis of *C. mosbachensis* being the descendant of *C. etruscus* and the ancestor of *C. lupus*, proposing instead *C. borjgali* as the probable ancestor of the *C. mosbachensis* lineage (Bartolini Lucenti et al., 2020). *Canis orcensis* from Venta Micena and *C. apolloniensis* from Apollonia-1 are two species that exhibit many similarities between them and differ little from *C. mosbachensis* or *C. borjgali*. In fact, Madurell- Malapeira et. al. (2021) dispute the attribution of *C. orcensis* and *C. apolloniensis* as different species and discusses the possible inclusion of both in *C. mosbachensis.*

The canid material from Tsiotra Vryssi presents some interesting peculiarities that contribute significantly to the previous discussion, even though they do not make a species attribution neither clearer nor easier. The *Canis* guild of TSR seems to be craniodentaly represented by three canid morphotypes; a sub-represented large one and two-medium sized ones; of the latter, the one being smaller. The postcranial elements additionally may support the presence of two canids.

The large-sized canid is represented by a single upper M1, TSR-46, that was first ascribed by Konidaris et al. (2015) to *C. etruscus* and consequently to as *Canis sp.* (Konidaris et al. 2021). The tooth does present proportions that are very close to the *C. etruscus* lectotype (MPM 47), but besides the more elevated protocone than paracone, does not display the same morphology, especially in the characters of the trigon and talon basins, which are not of the same depth as noted in *C. etruscus* (Cherin et al., 2014); the trigon basin is deeper while the talon one is reduced. Additionally, its metaconule is reduced to a crista-like form as it is described in the holotype of *C.* (*X.*) *lycaonoides* from Gombasek (Kretzoi, 1938) and does not possess a protoconule, features that according to Martínez-Navarro et al. (2021) characterize the primitive hypercarnivore *C.* (*X.*) *falconeri*. Its size is also larger, in contrasting with the rest of the *Canis* species (except for *C. etruscus*) and is closer to *Canis* (*Xenocyon*). Hence, we refer at the moment the larger canid from TSR to as *Canis* (*Xenocyon*) sp.

On both medium-sized canids from TSR the p3 alveoli lays lower in the mandible (probably not as low as in *C. borjgali* or *C. mosbachensis*), the mesial margin of the paraconid of m1 is distally inclined, the entoconid and the hypoconid of the m1 are connected with a sinuous transverse crest, the protoconid is larger than the metaconid in the m2, and they lack any of distolingual cuspids in the m2. Such common characters clearly differentiate the TSR canids from *C. arnensis* and place them closer to the group of *C. borjgali*, *C. orcensis*, *C. apolloniensis* and consequently to *C. mosbachensis*. *Canis etruscus* can also be excluded as a possible candidate since it differs in the elongated morphology of the nasals (ending well beyond the maxillofrontal suture), the same- depth figure of the M1 talon and trigon basins, and a vertical mesial margin of the m1 paraconid.

In many metric features, TSR-G20-11 is placed along with *C. accitanus* from Fonelas P-1, close to the range of *C. arnensis* and in cases was also grouped within the *C. mosbachensis* variability. *Canis arnensis* however can be excluded due to several morphological characteristics, discussed in the previous paragraph. *Canis accitanus* on the other hand, was recognized by Garrido and Arribas (2008) as a new species due to its morphological uniqueness and a rather small size. Brugal and Boudadi-Maligne (2011) doubt such an attribution and suggest the Fonelas P-1 taxon as proportionally belonging to *C. arnensis* since its features can be present in the variability of other canid populations. Bartolini Lucenti (2015) argues that it resembles *C. etruscus* in morphology, particularly in the cranial and upper dental appearance, but it also portrays dental similarities with the Dmanisi wolf. Some proportions (e.g., GNL/TL ratio) are also closer to *C. borjgali*. Martinez-Navarro et al. (2021) also propose that it could be a small-sized individual of *C. etruscus* which is present in the locality. Nevertheless, TSR-G20-11 differs from *C. accitanus* mostly in the M1 morphology, but if we follow the Brugal and Boudadi-Maligne (2011) proposition, these two taxa could belong together.

TSR-G20-11 compared to TSR-D17-37 is slenderer in most aspects, cranial, mandibular and dental ones and if they belong to the same species their differences would be explained by sexual dimorphism, which is present in *C. mosbachensis* (Sotnikova, 2001) but also in recent *Canis lupus* (e.g., Okarma and Buchalczyk, 1993; Hillis and Mallory, 1996; Trbojević and Ĉirović, 2016). Indeed, the smaller cranium does not possess a prominent sagittal crest, as observed in the larger one, however the outline of the nuchal crest is blunt on the smaller one and more triangular to the larger one. Additional morphological dental differences such the presence of diastemata, or the lack of a M1 protoconule on the size of the P4 protocone could be considered within the variability, and thus TSR-G20-11 could be just a small-sized individual of TSR-D17-37. Until their in between relationship is unraveled, the smaller TSR canid will be referred as *Canis* sp. (morphotype B).

Both in size and morphology the larger medium-sized TSR canid is most comparable to *C. borjgali* and *C. apolloniensis*; *C. orcensis* displays differentiation mostly in the M1 and dental proportions. Regarding *C. borjgali*, the character of the non-parallel medial walls of the tympanic bullae is questionable whether it occurs likewise in the TSR material, because of the fragmented portions. In TSR-D17-37, the deviation is visible, but probably not to the same degree as in the Dmanisi canid. *Canis apolloniensis* has overall a similar morphology with TSR-D17-37 but appears to present a more distinct lingual elongation of the protocone of the P4 and the two molars. The p3 alveoli of TSR-D17-37 are not very low in the mandible as in C. *borjgali* but are similar to the condition seen in *C. apollonensis*. Metrically, TSR-G17-37 is found in many cases within the *C. mosbachensis* and *C. borjgali* variability but not far from the *C. apolloniensis*. The selection of which diagnostic character would be more important than others in the discrimination among these taxa is not easy to make. For the time being, the larger medium-sized canid from TSR is attributed to *Canis borjgali* vel *apolloniensis*.

Comparison of the available postcranial remains from TSR also portray an important metrical and anatomical variance. The bones seem to belong to the range of *Canis* and are much smaller than those of *Canis* (*Xenocyon*). Although the previously discussed morphological differences among several postcranial elements of TSR cannot explicitly rule out (due to the scarcity of the material) the possibility of intraspecific variability, they seem likely to represent taxonomic differences at the species level.

5. Conclusion

Over the last years, the discovery of new species, new material, and the re-examination of old specimens, led to the modification of older taxonomic concepts, offering new interpretations regarding the taxonomy of the European *Canis* representatives. The rich and important material from TSR further contributes to the understanding of the European canids of the Early Pleistocene, especially in a critical period of time in the differentiation within the genus. The TSR fauna includes three canid taxa and their attribution takes into account the recent discoveries.

The large-sized canid is attributed to *Canis* (*Xenocyon*) sp. based on its general similarity in morphology and proportions with this taxon. This is the oldest record within the Mygdonia basin and may represent also its earliest occurrence in Greece.

The larger medium-sized canid displays similarities with two taxa that are closely related to the *Canis mosbachensis* lineage: *Canis borjgali* from Dmanisi and *Canis apolloniensis* from Apollonia-1. The slight differences that occur do not establish a clear species ascription, thus it is attributed to *Canis borjgali* vel *apolloniensis*. Nonetheless, the presence of *Canis borjgali* vel *apolloniensis* at TSR, documents the earliest record of this lineage in Greece, and perhaps in the southern Balkans.

The smaller, yet medium-sized canid has been attributed to *Canis* sp. (morphotype B). Its rather smaller size and some anatomic features do not contribute to its clear attribution, and its relationship with the larger medium-sized canid from TSR remains questionable at the moment.

The postcranial remains can be identified only to the genus level and portray a significant metrical and morphological variability. The bones seem to belong within the range of medium-sized *Canis* and are much smaller than known specimens of *Canis* (*Xenocyon*). The noted differences that have been discussed cannot exclude the possibility of intraspecific variability, nor can certainly result in two different species due to the scarcity of identified comparative material.

Further research and material enrichment, may resolve to the present complicated situation of the *Canis* guild from Tsiotra Vryssi.

References

Azzaroli, A., 1983. Quaternary mammals and the “End-Villafranchian” dispersal event—a turning point in the history of Eurasia. Palaeogeography, Palaeoclimatology, Palaeoecology 44, 117–139.

Bartolini Lucenti, S., 2015. A revision of Late Villafranchian dogs: Taxonomical relationships and implications for Early Pleistocene Canidae evolutionary history. Unpublished M.S. Thesis. Scienze e Tecnologie Geologiche, Universita degli Studi di Firenze, pp. 215.

Bartolini Lucenti, S., Rook, L., 2016. A review on the Late Villafranchian medium-sized canid *Canis arnensis* based on the evidence from Poggio Rosso (Tuscany, Italy). Quaternary Science Reviews 151, 58–71.

Bartolini Lucenti, S., Alba, D.M., Rook, L., Moyà-Solà, S., Madurell-Malapeira, J., 2017. Latest Early Pleistocene wolf-like canids from the Iberian Peninsula. Quaternary Science Reviews 162, 12–25.

Bartolini Lucenti, S., Bukhsianidze, M., Martínez-Navarro, B., Lordkipanidze, D., 2020. The wolf from Dmanisi and Augmented Reality: review, implications, and opportunities. Frontiers in Earth Science 8, 131.

Bartolini Lucenti, S., Madurell-Malapeira, J., Martínez-Navarro, B., Palmqvist, P., Lordkipanidze, D., Rook, L., 2021. The early hunting dog from Dmanisi with comments on the social behaviour in Canidae and hominins. Scientific reports, 11, 13501.

Bellani, G. G., 2020. Order of carnivores (Carnivora). Felines of the World, 1–12.

Biknevicius A. R., Van Valkenburgh B., 1996. Design for killing: craniodental adaptations of predators. In: Gittleman, J. (Ed.), Carnivore behavior, ecology, and evolution, Volume 2. John Hopkins University Press, 393–428.

Bonifay, M.F., 1971. Carnivores Quaternaires du Sud-Est de la France. Mémoires du Muséum National d’Histoire Naturelle, Nev. Série C 21, 1–377.

Boudadi-Maligne, M., 2010. Les *Canis* Pleistocenes du Sud de la France: Approche Biosystematique, Evolutive et Biochronologique. Archéologie et Préhistoire. Université Bordeaux 1. Français. pp. 412.

Brugal, J.P., Boudadi-Maligne, M., 2011. Quaternary small to large canids in Europe: Taxonomic status and biochronological contribution. Quaternary International 243, 171–182.

Cherin, M., Bertè, D.F., Rook, L., Sardella, R., 2014. Re-defining *Canis etruscus* (Canidae, Mammalia): A new look into the evolutionary history of Early

Pleistocene dogs resulting from the outstanding fossil record from Pantalla (Italy). Journal of Mammal Evolution 21, 95–110.

Crusafont Pairo, M., 1950. El primer representante del género *Canis* en el Pontiense eurasiatico (*Canis cipio* nova sp.). Boletín de la Real Sociedad Española de Historia Natural (Geologia) 48, 43–51.

Del Campana, D., 1913. I cani pliocenici di Toscana. Tipografia successori fratelli Nistri.

Fischer von Waldheim, G., 1817. Adversaria zoologica. Mémoires de la Société impériale des naturalistes de Moscou, 5, 357–472.

Forsyth-Major, C. I., 1877. Considerazioni sulla fauna dei mammiferi pliocenici e post-pliocenici della Toscana. Atti della Società Toscana di scienze naturali, Memorie, 3, 207–227.

Garrido, G., 2008. El registro de *Vulpes alopecoides* (Forsyth-Major, 1877), *Canis etruscus* Forsyth-Major, 1877 y *Canis* cf. *falconeri* Forsyth-Major, 1877 (Canidae, Carnivora, Mammalia) en Fonelas P-1 (Cuenca de Guadix, Granada). In A. Arribas (Ed.), Vertebrados del Plioceno superior terminal en el suroeste de Europa: Fonelas P-1 y el Proyecto Fonelas. Cuadernos del Museo Geominero, nº 10. Instituto Geológico y Minero de España, Madrid, 159–186.

Garrido, G., Arribas, A., 2008. *Canis accitanus* nov. sp., a new small dog (Canidae, Carnivora, Mammalia) from the Fonelas P-1 Plio-Pleistocene site (Guadix basin, Granada, Spain). Geobios 41, 751–761.

Giusti, D., Konidaris, G.E., Tourloukis, V., Marini, M., Maron, M., Zerboni, A., Thompson, N., Koufos, G.D., Kostopoulos, D.S., Harvati, K., 2019. Recursive anisotropy: a spatial taphonomic study of the Early Pleistocene vertebrate assemblage of Tsiotra Vryssi, Mygdonia Basin, Greece. Boreas 48, 713–730.

Gopalakrishnan, S., Sinding, M.H.S., Ramos-Madrigal, J., Niemann, J., Samaniego Castruita, J.A., Vieira, F.G., Carøe, C., Montero, M. de M., Kuderna, L., Serres, A., Gonzalez-Basallote, V.M., Liu, Y.H., Wang, G.D., Marques-Bonet, T., Mirarab, S., Fernandes, C., Gaubert, P., Koepfli, K.P., Budd, J., Rueness, E.K., Heide Jørgensen, M.P., Petersen, B., Sicheritz-Ponten, T., Bachmann, L., Wiig, Ø., Hansen, A.J., Gilbert, M.T.P., 2018. Interspecific gene flow shaped the evolution of the genus *Canis*. Current Biology 28, 3441–3449.

Hammer, Ø., Harper, D.A.T., Ryan, P.D., 2001. PAST: Paleontological statistics software package for education and data analysis. Palaeontologia Electronica 4, 9.

Hillis, T.L., Mallory, F.F., 1996. Sexual dimorphism in wolves (*Canis lupus*) of the Keewatin District, Northwest territories, Canada. Canadian Journal of Zoology, 74(4), 721-725.

Kockel, F., Mollat, H., Walther, H.W., 1977. Erläuterungen zur geologischen Karte der Chalkidiki und angrenzender Gebiete 1:100.000 (Nord-Griechenland). Bundesanstalt für Geowissenschaften und Rohstoffe, Hannover, 1–119.

Konidaris, G.E., Kostopoulos, D.S., Maron, M., Schaller, M., Ehlers, T.A., Aidona, E., Marini, M., Tourloukis, V., Muttoni, G., Koufos, G.D., Harvati, K., 2021. Dating of the Lower Pleistocene vertebrate site of Tsiotra Vryssi (Mygdonia Basin, Greece): Biochronology, Magnetostratigraphy, and Cosmogenic Radionuclides. Quaternary 4, 1.

Konidaris, G.E., Tourloukis, V., Kostopoulos, D.S., Thompson, N., Giusti, D., Michailidis, D., Koufos, G.D., Harvati, K., 2015. Two new vertebrate localities from the Early Pleistocene of Mygdonia Basin (Macedonia, Greece): Preliminary results. Comptes Rendus - Palevol 14, 353–362.

Koufos, G. D., Syrides, G. E., Kostopoulos, D. S., Koliadimou K. K., 1995. Preliminary results about the stratigraphy and the palaeoenvironment of Mygdonia Basin, Macedonia, Greece. Geobios, M.S. 18, 243–249.

Koufos, G., 2018. New Material and Revision of the Carnivora, Mammalia from the Lower Pleistocene Locality Apollonia 1, Greece. Quaternary 1, 6.

Koufos, G.D., 1992. The Pleistocene carnivores of the Mygdonia basin (Macedonia, Greece). Annales de Paléontologie 78, 205–257.

Koufos, G.D., 2001. The Villafranchian mammalian faunas and biochronology of Greece. Bollettino della Societa Paleontologica Italiana 40, 217–223.

Koufos, G.D., Kostopoulos, D.S., 1997. New Carnivore material from the Plio-Pleistocene of Macedonia, Greece with the description of a new canid. München Geowiss. Abh., 34, 33–63.

Koufos, G.D., Konidaris, G.E., Harvati, K., 2018. Revisiting *Ursus etruscus* (Carnivora, Mammalia) from the Early Pleistocene of Greece with description of new material. Quaternary International 497, 222–239.

Koufos, G.D., Syrides, G.E., Kostopoulos, D.S., Koliadimou, K.K., 1995. Preliminary results about the stratigraphy and the palaeoenvironment of Mygdonia Basin, Macedonia, Greece. Geobios 28, 243–249.

Kurtén, B., 1974. A history of coyote-like dogs (Canidae, Mammalia). Acta Zoologica Fennica 140, 1–38.

Lacombat, F., Abbazzi, L., Ferretti, M.P., Martínez-Navarro, B., Moullé, P.E., Palombo, M.R., Rook, L., Turner, A., Valli, A.M. F., 2008. New data on the Early Villafranchian fauna from Vialette (Haute-Loire, France) based on the collection of the Crozatier Museum (Le Puy-en-Velay, Haute-Loire, France). Quaternary International 179, 64–71.

Madurell-Malapeira, J., Bartolini-Lucenti, S., Prat-Vericat, M., Sorbelli, L., Blasetti, A., Ferretti, M. P., Goro, A., Cherin, M., 2021. Jaramillo-aged carnivorans from Collecurti (Colfiorito Basin, Italy). Historical Biology, 1–13.

Martínez-Navarro, B., Rook, L., 2003. Gradual evolution in the African hunting dog lineage systematic implications. Comptes Rendus Palevol 2, 695–702.

Martínez-Navarro, B., Belmaker, M., Bar-Yosef, O., 2009. The large carnivores from 'Ubeidiya (early Pleistocene, Israel): biochronological and biogeographical implications. Journal of Human Evolution 56, 514–524.

Martínez-Navarro, B, 2010. Early Pleistocene faunas of Eurasia and hominin dispersals. In: Fleagle JG, Shea JJ, Grine FE, Baden AL, Leakey RE (Eds) Out of Africa I. The First Hominin Colonization of Eurasia. Springer Verlag. Vertebrate Paleobiology and Paleoanthropology Series, 207–224.

Martínez-Navarro, B., Lucenti, S.B., Palmqvist, P., Ros-Montoya, S., Madurell-Malapeira, J., Espigares, M.P., 2021. A new species of dog from the Early Pleistocene site of Venta Micena (Orce, Baza Basin, Spain). Comptes Rendus Palevol, 20, 297–314.

Miller, M.E., Christensen, G.C., Evans, H.E., 1964. Anatomy of the dog. W.B. Saunders Company, Philadelphia, pp. 941.

Mosimann, J.E., 1970. Size allometry: size and shape variables with characterizations of the lognormal and generalized gamma distributions. Journal of the American Statistical Association 65, 930–945.

Okarma, H., Buchalczyk, T., 1993. Craniometrical characteristics of wolves *Canis lupus*. Acta Theriologica, 38(3), 253-262.

Petrucci, M., Cipullo, A., Martínez-Navarro, B., Rook, L., Sardella, R., 2013. The Late Villafranchian (Early Pleistocene) carnivores (Carnivora, Mammalia) from Pirro Nord (Italy). Palaeontographica 298, 113–145.

Psilovikos, A.A., 1977. Palaeogeographic development of the basin and lake of Mygdonia (Langada-Volvi area), Greece. Aristotle University of Thessaloniki, Thessaloniki, 1–156.

Rook L., 1993. I cani dell'Eurasia dal Miocene Superiore al Pleistocene Medio. Unpublished doctoral thesis, Modena-Bologna-Firenze and Roma "La Sapienza" Universities, 1–154.

Sardella, R., Palombo, M.R., 2007. The Pliocene-Pleistocene boundary: Which significance for the so called "wolf event"? Evidences from Western Europe. Quaternaire 18, 65–71.

Sardella, R., Bertè, D., Iurino, D.A., Cherin, M., Tagliacozzo, A., 2014. The wolf from Grotta Romanelli (Apulia, Italy) and its implications in the evolutionary history of Canis lupus in the Late Pleistocene of Southern Italy. Quaternary International 328–329, 179–195.

Sillero-Zubiri, C., 2009. Family Canidae. In D. E. Wilson & R. A. Mittermeier (Eds.), Handbook of the mammals of the world. Vol. 1. Carnivores. Barcelona, Spain: Lynx Ediciones 352–446.

Simpson, G. G., 1941. Large Pleistocene felines of North America. American Museum Novitates 1136, 1–27.

Simpson, G. G., Roe, A., Lewontin, R. C., 1960. Quantitative Zoology. Harcourt Brace, New York.

Soergel, W., 1925. Die Säugetierfauna des altdiluvialen Tonlages von Jockgrim in des Pfalz. Zeitschrift der Deutischen Geologischen Gesellschaft 77, 405–438.

Sotnikova, M.V., 2001. Remains of Canidae from the lower Pleistocene site of Untermassfeld. In: Kahlke, R.D. (Ed.), Das Pleistozän von Untermassfeld bei Meiningen (Thüringen) Teil. 2. Habelt Verlag, Bonn, 607–632.

Sotnikova, M., Rook, L., 2010. Dispersal of the Canini (Mammalia, Canidae: Caninae) across Eurasia during the Late Miocene to Early Pleistocene. Quaternary International 212, 86–97.

Tedford, R.H., Wang, X., Taylor, B.E., 2009. Phylogenetic systematics of the North American fossil Caninae (Carnivora: Canidae). Bulletin of the American Museum of Natural History, 1–218.

Thenius, E., 1954. Die Caniden (Mammalia) aus dem Altquartär von Hundsheim (Niederösterreich) nebst Bemerkugen zur Stammesgeschichre der Gattung *Cuon*. Neues Jahrbuch für Geologie und Paläontologie, Abhandlungen 99, 230–286.

Torre, D., 1967. I cani villafranchiani della Toscana. Paleontographia Italica 64, 113–138.

Trbojević, I., Ćirović, D., 2016. Sexual dimorphism and population differentiation of the wolf (*Canis lupus*) based on morphometry in the Central Balkans. North-Western Journal of Zoology, 12(2).

Tsoukala, E., Chatzopoulou, K., 2005. A new Early Pleistocene (Latest Villafranchian) site with Mammals in Kalamotó (Mygdonia Basin, Macedonia, Greece) -

Preliminary Report. Mitteilungen der Kommission für Quartärforschung der Österreichischen Akademie der Wissenschaften 14, 213–233.

Vekua, A., 1995 - Die Wirbeltierfauna des Villafranchium von Dmanisi und ihre biostratigraphishe Bedeutung. Jahrbuch des Römisch-Germanischen Zentralmuseums Mainz 42, 77–180.

Wang, X., Tedford, R.H., 1994. Basicranial anatomy and phylogeny of primitive canids and closely related miacids (Carnivora: Mammalia). American Museum Novitates 3092, 1–34.

Wang, X., Tedford, R.H., 2007. Evolutionary history of canids. In: Jensen, P. (Ed.), 2007. The Behavioral Biology of Dogs, Volume 1, 3–10.

Wang, X., Tedford, R.H., 2008. Dogs: Their fossil relatives and evolutionary history. Columbia University Press, New York, pp. 219.

Wang, X., Tedford, R.H., Van Valkenburgh, B., Wayne, R.K., 2004. Evolutionary history, molecular systematics, and evolutionary ecology of Canidae. In: Macdonald, D.W., Sillero Zubiri, C., (Eds.), 2004. Biology and conservation of wild canids. Oxford University Press, Oxford, United Kingdom, 37–54.

Zrzavý, J., Duda, P., Robovský, J., Okřinová, I., Pavelková Řičánková, V., 2018. Phylogeny of the Caninae (Carnivora): Combining morphology, behaviour, genes and fossils. Zoologica Scripta, 47.

Appendix I

Table 5. Cranial measurements of the *Canis borjgali* vel *apolloniensis* (TSR-D17-37a) and *Canis* sp. (morphotype B) (TSR-G20-11a) from TSR, given in mm. Values in brackets are not precise.

Specimen	AB	BL	CBL	Ect	ECW	Eu	FL	GNL	GPW	GWOC	NcL	PL	POCW	SCL	SH	TL	Zyg	PS	BS	LCR	LMR	LPR
TSR-G20-11a	44.4	164	171.15	[46.44]	[26.12]	[55.1]	104	[66]	[52.1]	32.7	86.01	93.32	[37.5]	[86.1]	[49]	[184.1]	[91.01]	35.12	129.1	66.12	19.09	49.56
TSR-D17-37a	43.83	165.3	[173.5]	[43.91]	[33.84]	[65.36]	113.5	[76.13]	58.9	[38.7]	[83.1]	[95.71]	[39.3]	[99.2]	50.75	192.1	[99.9]	47.81	130.1	70.42	21.2	53.55

Table 6. Mandibular measurements of the *Canis borjgali* vel *apolloniensis* (TSR-D17-37b; TSR-F14-2; TSR-H20-1) and *Canis* sp. (morphotype B) (TSR-G20-11b) from TSR, given in mm. Values in brackets are not precise.

Specimen		TL	LLCR	LLPR	LLMR	HR	LAP	Mm1H	Mp2H	Mp4H
TSR-G20-11b	Right	129.5	75.45	40.67	33.69			20.1	15.45	19.79
TSR-D17-37b	Right	135.72	79.08	42.47	36.02	[49.9]	134.59	20.55	16.68	20.55
TSR-D17-37b	Left	136.41	79.16	42.28	35.89	[50.21]	133.68	20.32	17.44	20.8
TSR-F14-2	Right		80.14	[43.39]	36.18	[49.45]		22.85	19.87	22.45
TSR-H20-1	Right				39.72	55.95		21.92		21.78

Table 7. Upper teeth measurements of the *Canis borjgali* vel *apolloniensis* (TSR-D17-37a; TSR-G16-46; TSR-G16-29; TSR-D16-14; TSR-D17-42; TSR-C15-13; TSR-E22-6), *Canis* sp. (morphotype B) (TSR-G20-11a; TSR-G20-11e; TSR-G20-11c; TSR-G20-11d) and *Canis* (*Xenocyon*) sp. (TSR-46) from TSR, given in mm.

Specimen		**I1 L**	**I1 W**	**I2 L**	**I2 W**	**I3 L**	**I3 W**	**C L**	**C W**	**P1 L**	**P1 W**	**P2 L**	**P2 W**	**P3 L**	**P3 W**	**P4 L**	**P4 W**	**M1 L**	**M1 W**	**M2 L**	**M2 W**
TSR-D17-37a	Right	5.45	5.45	6.07	6.6	7.71	5.86	10.25	6.03	6.79	4.81	11.6	5.1	13.17	5.52	21.1	10.77	14.29	16.5	6.92	10.14
TSR-D17-37a	Left	5.5	5.5	6.15	6.46	7.8	5.85			6.84	4.89	11.45	5.09		5.42	21.25	10.55	14.2	16.38	6.93	10
TSR-G20-11a	Right					6.5	5.05	8.6	5.16	5.72	3.45	9.15	3.84	10.61	4.24	18.6	8.4	12.55	14.36	7.3	10.1
TSR-G20-11a	Left											9.05	3.8	10.65	4.32	18.62	8.32	12.57	14.39	7.25	10.05
TSR-G16-46	Left											10.32	4.21	12.5	4.6			13.4	16.26	6.62	10.79
TSR-46	Right																	16.42	19.4		
TSR-G16-29	Right															19.78	10.14				
TSR-D16-14	Left															20.3					
TSR-D14-7	Right																			8	10.9
TSR-G20-11e	Left					5.7	4.52														
TSR-G20-11c	Left			4.3	4.97																
TSR-G20-11d	Right							7.95	4.85												
TSR-D17-42	Left							9.51	5.99												
TSR-C15-13	Right							7.53	4.95												
TSR-E22-6	Left			5.85	5.67																

Table 8. Lower teeth measurements of the *Canis borjgali* vel *apolloniensis* (TSR-D17-37b; TSR-F14-2; TSR-H20-1) and *Canis* sp. (morphotype B) (TSR-G20-11b) from TSR, given in mm.

Specimen		**i1**		**i2**		**i3**		**c**		**p1**		**p2**		**p3**		**p4**		**m1**		**tdm1**		**trm1**		**m2**		**m3**	
		L	**W**	**L**	**W**	**L**	**W**	**L**	**W**	**L**	**W**	**L**	**W**	**L**	**W**	**L**	**W**	**L**	**W**	**L**	**W**	**L**	**W**	**L**	**W**	**L**	**W**
TSR-F14-2	Right									5.49	3.82	10.34	4.5			13.8	6.49	21.62	8.76	6.87	7.98	14.2	8.35				
TSR-H20-1	Left																	23.2	9.48	9.9	9.2	14.1	9.27	10.36	7.48		
TSR-D17-37b	Right	3.85	3	5.23	4.4	5.6	5.6	9.41	6.8	5.18	4.53	10.73	5.16	12.4	5.6	14.36	6.8	23.4	9.21	7.2	8.8	15.67	8.98	10.07	7.1	5.09	4.66
TSR-D17-37b	Left	3.9	3.25	5.35	4.36	5.64	5.65	9.4	6.88	5.5	4.34	10.74	5.15	12.66	5.7	14.3	6.8	23.39	9.16	7.21	8.75	15.8	9.01	9.94	7.2	5.17	4.76
TSR-G20-11b	Right							8.07	5.5			8.93	4.08	10.45	4.42	11.76	5.41	20.84	7.8	7.45	7.75	13.26	6.96	9.58	6.12		

Table 9. Measurements of scapula and vertebrae; axis and sacrum of *Canis* sp. from TSR, given in mm.

	Specimen		**SLC**	**GLP**	**LG**	**WG**	**LAP**	**SBV**	**WFacr**	**WPtr**	**HFcr**	**WFtcr**
Scapula	**TSR-H18-22**	Right	23.03	27.62	22.82	16.27						
Scapula	**TSR-G20-10a**	Right	20.08	25.62	20.06	14.1						
Axis	**TSR-G17-30**	-					42.7	17.38	24.11	30.51		
Sacrum	**TSR-G18-41**	-									9.91	18.99

Table 10. Measurements of the postcranial elements; humerus, radius, ulna, tibia, femur, calcaneus and astragalus of *Canis* sp. from TSR, given in mm. Values in brackets are not precise.

	Specimen		GL	GLC	SD	AD	WD	AP	WP	SAD	SDO	DPA	WPC	HA	SW
Humerus	**TSR-D18-90**	Right		151.8	10.82			37.42							
Humerus	**TSR-D18-93**	Left			11.81										
Humerus	**TSR-H18-27**	Right	153.8	149.85	11.82		26.74	37.49		12.23					
Humerus	**TSR-H18-15**	Left			[11.2]		26.1	30.40		10.16					
Humerus	**TSR-G20-10b**	Right		143.45	10.12		20.10			10.42					
Humerus	**TSR-H22-12**	Left	155.72	150.0	10.40			36.71							
Radius	**TSR-G21-86**	Right	142.93		11.11	10.79	20.22	9.17	14.34						
Radius	**TSR-D18-91**	Right							15.13						
Radius	**TSR-D18-92**	Left	[147]		11.15		[21.63]	10.7	16.41						
Radius	**TSR-H22-8a**	Left					23.20								
Ulna	**TSR-D18-91**	Left									17.50	22.97	16.18	21.60	
Ulna	**TSR-H22-8b**	Left									16.63				
Ulna	**TSR-G20-44**	Right									16.32	19.85	13.61	19.06	
Tibia	**TSR-C18-17**	Right			11.53										
Femur	**TSR-C18-17**	Right			11.4										
Calcaneus	**TSR-C18-17**	Right	41.10												[9.31]
Calcaneus	**TSR-C18-17**	Left	42.16												8.93
Astragalus	**TSR-C18-17**	Left	24.13				10.13								7.84

Table 11. Measurements of the metapods; metacarpals (Mc) and metatarsals (Mt), of *Canis* sp. from TSR, given in mm.

	Specimen		GL	WS	WD	AD
Mc1	**TSR-G20-10g**	Left	20.68	3.97	5.63	4.81
Mc1	**TSR-H21-5**	Left		4.09	5.71	
Mc2	**TSR-G20-10d**	Left	53.81	5.64	7.64	7.13
Mc2	**TSR-F14-11**	Right		5.23	7.65	8.04
Mc3	**TSR-G20-10f**	Left	62.16	5.29		
Mc3	**TSR-G20-32**	Right	61.42	5.31	7.69	7.41
Mc4	**TSR-G20-10e**	Left	63.19	5.25	7.14	7.32
Mc5	**TSR-G20-10c**	Left		5.93		
Mt2	**TSR-C18-17**	Right	64.46	5.69	7.69	7.91
Mt2	**TSR-C18-17**	Left		5.63		
Mt3	**TSR-C18-17**	Right	70.51	6.2	7.26	8.45
Mt3	**TSR-C18-17**	Left		6.35		
Mt4	**TSR-C18-17**	Right	70.71	5.46	6.82	8.19
Mt4	**TSR-F21-7**	Left		5.96		
Mt4	**TSR-C18-17**	Left		5.69		
Mt5	**TSR-C18-17**	Right	64.22	4.43	6.81	7.72
Mt5	**TSR-C18-17**	Left	64.72	4.98	7.18	7.91
Mt5	**TSR-F20-44**	Left		4.63	6.67	6.98

Table 12. Measurements of the phalanges; proximal (Ph1) and medial (Ph2), of *Canis* sp. from TSR, given in mm.

	Specimen		GL	WS	WD	AD	WP	AP
Mc2 Ph1	**TSR-G20-10d**	Left	20.34	4.78	6.01	4.83	7.69	6.75
Mc3 Ph1	**TSR-G20-10f**	Left	23.65	4.26	5.87	5.06	7.26	7.21
Mc4 Ph1	**TSR-G20-10e**	Left	23.64	4.37	6.07	4.98	7.39	6.96
Mc5 Ph1	**TSR-G20-10c**	Left		4.56				
Mc3 Ph2	**TSR-G20-10f**	Left	17.05	4.49	6.77	4.58	6.68	6.03
Mc4 Ph2	**TSR-G20-10e**	Left	17.31	4.27	6.63	4.48	6.42	5.74
Mp2 Ph1	**TSR-C18-17**	Right	21.64	4.46	6.33	4.68	8.19	6.94
Mp3 Ph1	**TSR-C18-17**	Right	25.63	4.41	6.42	4.9	7.71	7.05
Mp4 Ph1	**TSR-C18-17**	Right	25.19	4.37	6.19	4.7	7.67	6.88
Mp5 Ph1	**TSR-C18-17**	Right	20.98	3.96	6.11	4.55	7.49	6.51
Mp2 Ph2	**TSR-C18-17**	Right	12,07	5.38	6.39	4.56	7.16	5.52
Mp3 Ph2	**TSR-C18-17**	Right	17.32	3.95	6.65	4.5	6.97	5.75
Mp4 Ph2	**TSR-C18-17**	Right	17.34	4.29	6.41	4.45	6.93	5.43
Mp5 Ph2	**TSR-C18-17**	Right	12.02	5.1	6.32	4.39	6.98	5.03

Table 13. Measurements of the unidentified phalanges; proximal (Ph1) and medial (Ph2), of *Canis* sp. from TSR, given in mm.

	Specimen	GL	WS	WD	AD	WP	AP
Ph1	**TSR-G21-76**	20.34	4.73	6.09	4.88	7.54	6.76
Ph1	**TSR-G20-38**	19.84	4.56	6.19	4.83	8.06	6.75
Ph1	**TSR-C17-44**	21.87	4.72	6.44	4.83	8.4	7.25
Ph1	**TSR-F16-31**	16.21	3.56	4.58	3.87	5.98	4.86
Ph1	**TSR-G16-9**	25.87	4.71	6.41	5.02	7.74	7.59
Ph1	**TSR-H22-10a**	21.13	4.88	6.41	4.86	7.95	7.55
Ph1	**TSR-H22-10b**	25.19	5.09	6.46	4.91	7.93	7.87
Ph1	**TSR-H22-10c**		5.04			8.05	7.59
Ph1	**TSR-H22-10d**					7.67	6.98
Ph1	**TSR-H22-10e**			6.04	4.46		
Ph2	**TSR-E21-60**	18.61	4.48	6.22	4.28	6.41	5.43
Ph2	**TSR-F14-8**	14.28	5.35	6.48	4.66	7.26	6.26
Ph2	**TSR-48b**					7.38	7.57
Ph2	**TSR-F15-6**	17.48	4.54	6.86	4.55	6.66	6.13
Ph2	**TSR-H22-10f**	17.94	4.66	6.41	4.77	7.17	6.15
Ph2	**TSR-H22-10g**	18.09	4.61	6.44	4.74	7.29	6.11
Ph2	**TSR-H22-10h**					7.34	5.25

Appendix II

Plate I. *Canis borjgali* vel *apolloniensis* from Tsiotra Vryssi. Scale bar: 2cm.

1. TSR-D17-37a, cranium: **a.** dorsal view; **b.** left lateral view; **c.** ventral view; **d.** right lateral view.

2. TSR-D17-37b, mandible: **a.** occlusal view; **b.** right lateral view; **c.** left lateral view.

Pl. I

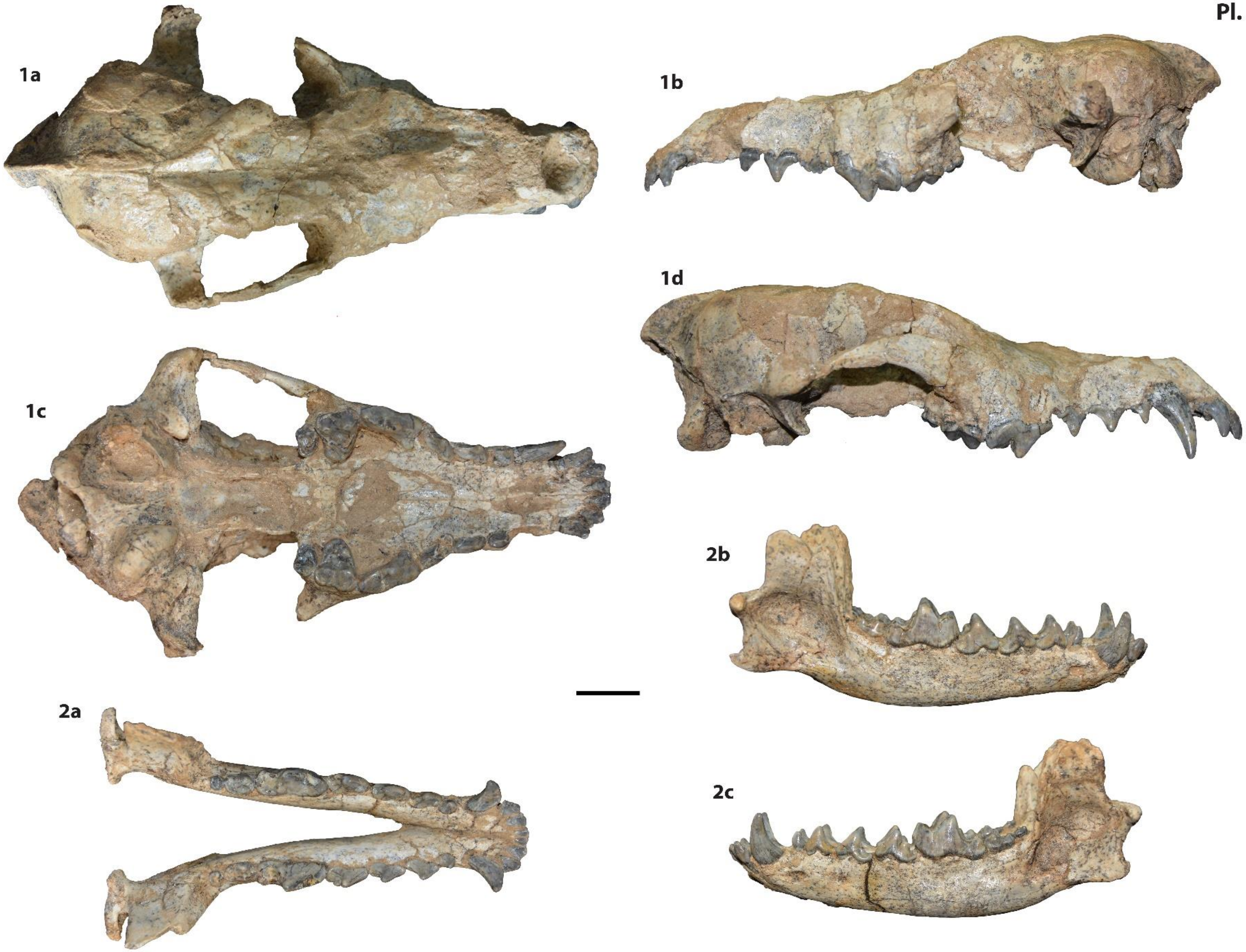

Plate II. *Canis* sp. (morphotype B) from Tsiotra Vryssi. Scale bar: 2cm.

1. TSR-G20-11a, cranium: **a**. dorsal view; **b**. left lateral view; **c**. ventral view; **d**. right lateral view.

2. TSR-G20-11b, right hemimandible: **a**. occlusal view; **b**. buccal view; **c**. lingual view.

3. TSR-G20-11c, left I2: **a**. buccal view; **b**. lingual view.

4. TSR-G20-11e, left I3: **a**. buccal view; **b**. lingual view.

5. TSR-G20-11d, right C: **a**. buccal view; **b**. lingual view.

Pl. II

1a

1b

1c

1d

2a

2b

2c

3a

4a

5a

3b

4b

5b

Plate III. *Canis borjgali* vel *apolloniensis* (1–8, 10); *Canis* (*Xenocyon*) sp. (9) from Tsiotra Vryssi. Scale bar: 2cm.

1. TSR-H20-1, left hemimandible: **a**. lateral view; **b**. medial view; **c**. occlusal view.

2. TSR-F14-2, right hemimandible: **a**. lateral view; **b**. medial view; **c**. occlusal view.

3. TSR-G16-46, left maxillary fragment: **a**. lateral view; **b**. occlusal view.

4. TSR-D16-14, left P4: **a**. lingual view; **b**. buccal view.

5. TSR-G16-29, right P4: **a**. lingual view; **b**. buccal view; **c**. occlusal view.

6. TSR-C15-13, right C, lingual view.

7. TSR-D17-42, left C, lingual view.

8. TSR-E22-6, left I3, buccal view.

9. TSR-46, right M1, occlusal view.

10. TSR-D14-7, right M2, occlusal view.

Pl. III

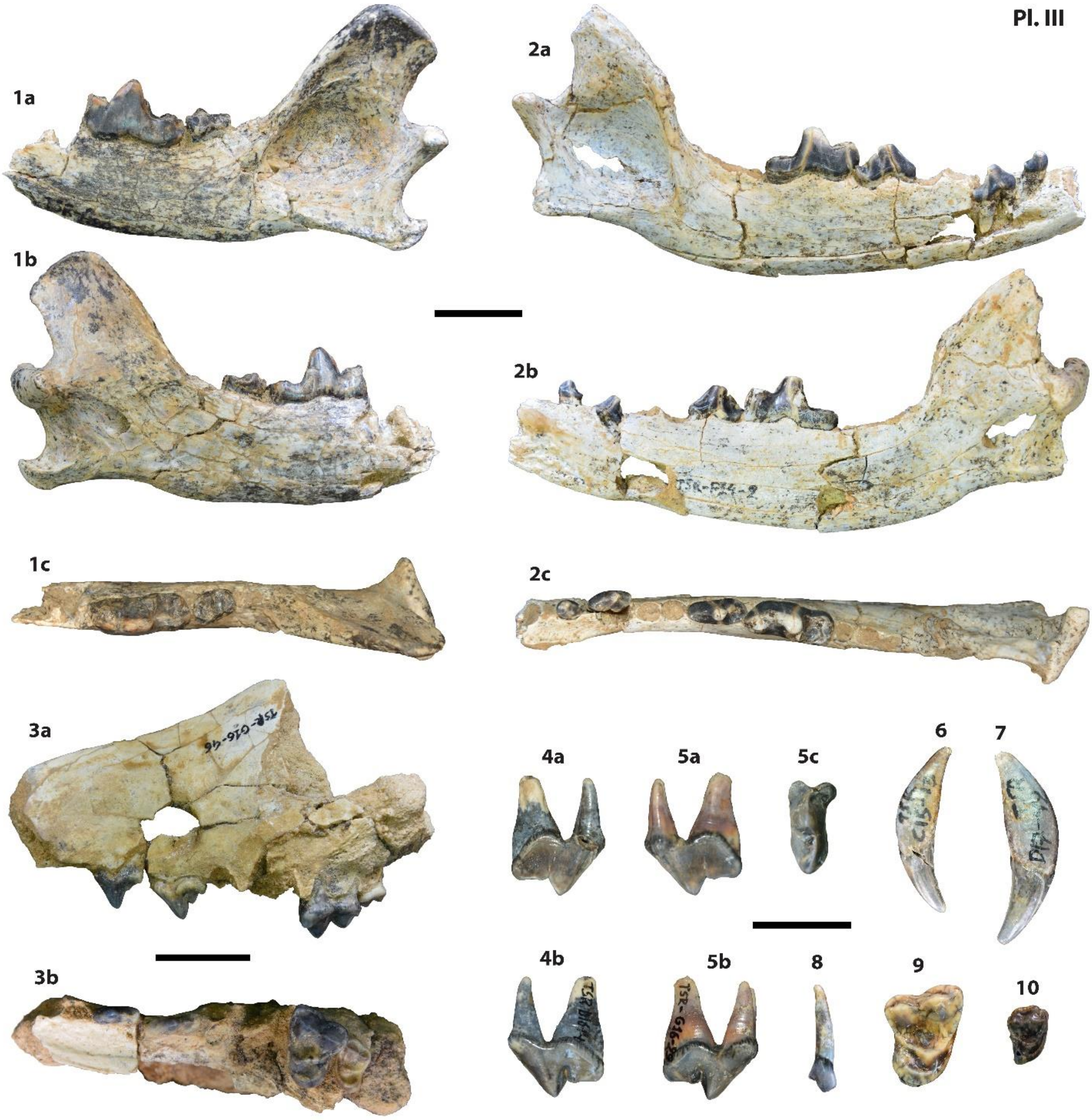

Plate IV. Postcranial elements of *Canis* sp. from Tsiotra Vryssi Scale bar: 3cm.

1. TSR-G20-10b, right humerus: **a**. anterior view; **b**. lateral view; **c**. posterior view; **d**. medial view.

2. TSR-G20-10a, right scapula: **a**. distal view; **b**. anterior view.

3. Left fore foot, anterior view: **a**. TSR-G20-10g, Mc1; **b**. TSR-G20-10d, Mc2 with proximal phalanx; **c**. TSR-G20-10f, Mc3 with proximal, medial and distal Phs; **d**. TSR-G20-10e, Mc4 with proximal, medial and distal Phs; **e**. TSR-G20-10c, Mc5 with proximal, medial and distal Phs.

4. TSR-H18-22, right scapula: **a**. distal view; **b**. anterior view.

5. TSR-G17-30, axis with C3: **a**. dorsal view; **b**. lateral view.

6. TSR-G18-41, sacrum, dorsal view.

7. TSR-H18-27, right humerus: **a**. anterior view; **b**. lateral view; **c**. posterior view; **d**. medial view.

8. TSR-H18-15 left humerus **a**. posterior view; **b**. medial view; **c**. anterior view.

Pl. IV

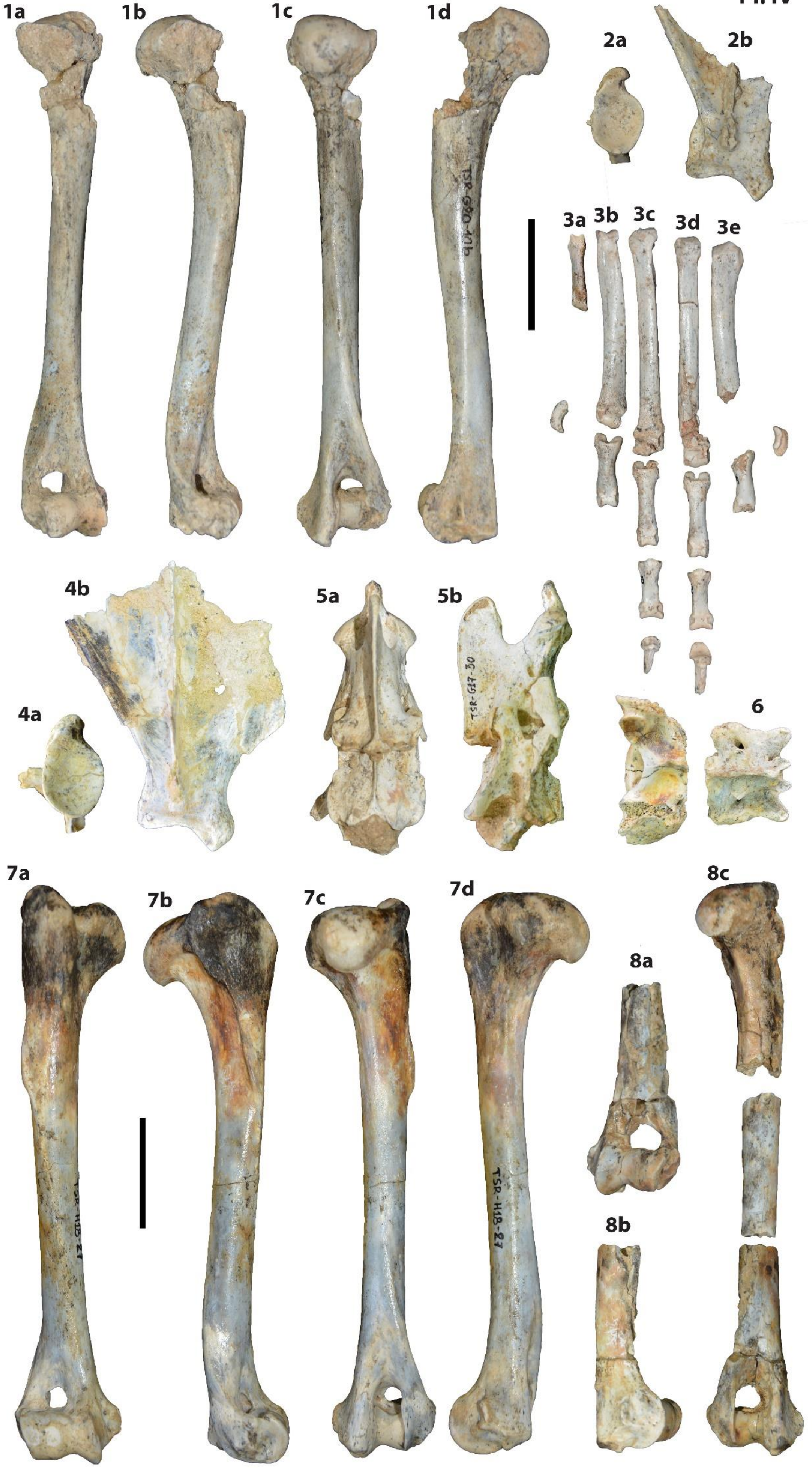
1a
1b
1c
1d
TSR-G20-101b
2a
2b
3a
3b
3c
3d
3e
4b
4a
5a
5b
TSR-G17-30
6
7a
7b
7c
7d
TSR-H18-27
TSR-H18-27
8a
8b
8c

Plate V. Postcranial elements of *Canis* sp. from Tsiotra Vryssi Scale bar: 3cm.

1. TSR-G20-44, right ulna: **a**. lateral view; **b**. anterior view; **c**. medial view.

2. TSR-G21-86, right radius: **a**. posterior view; **b**. lateral view; **c**. anterior view; **d**. medial view; **e**. proximal view; **f**. distal view.

3. TSR-D18-91, right radius: **a**. anterior view **b**. posterior view.

4. TSR-D18-91, left ulna: **a**. medial view; **b**. anterior view; **c**. lateral view.

5. TSR-D18-90, right humerus, posterior view.

6. TSR-D18-93, left humerus, posterior view.

7. TSR-D18-92, left radius: **a**. posterior view; **b**. anterior view; **c**. proximal view.

Pl. V

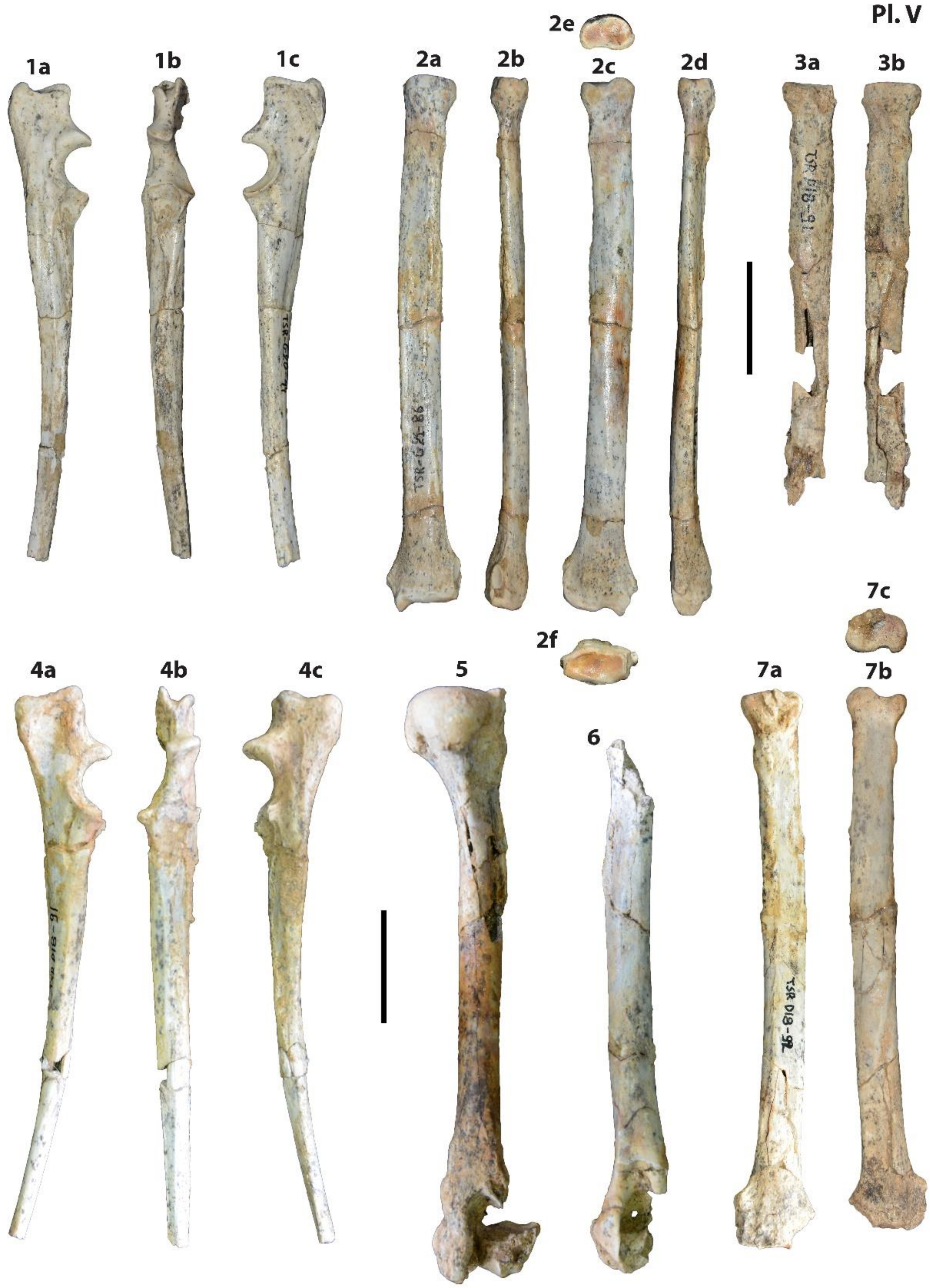

Plate VI. Postcranial elements of *Canis* sp. from Tsiotra Vryssi Scale bar: 3cm.

1. TSR-C18-17, pelvis, lumbar and caudal vertebrae: dorsal view.

2. TSR-C18-17, right femur, posterior view.

3. TSR-C18-17, right tibia: **a**. lateral view; **b**. anterior view; c. medial view.

4. TSR-C18-17, left calcaneus: a. medial view; **b**. anterior view; **c**. lateral view; **d**. posterior view.

5. TSR-C18-17, right calcaneus: **a**. posterior view; **b**. anterior view.

6. TSR-C18-17, left astragalus: **a**. anterior view; **b**. posterior view.

7. TSR-C18-17 (hind foot) right metatarsals (1–5) with proximal, medial and distal phs, anterior view.

8. TSR-C18-17 left metatarsals (1–5), anterior view.

Pl. VI

1

3a **3b** **3c**

2

4a **4b** **4c** **4d**

5a **5b**

6a **6b**

7

8